

# DeepCorrect: Correcting DNN Models against Image Distortions

Tejas Borkar  
Arizona State University  
tsborkar@asu.edu

Lina Karam  
Arizona State University  
karam@asu.edu

## Abstract

*In recent years, the widespread use of deep neural networks (DNNs) has facilitated great improvements in performance for computer vision tasks like image classification and object recognition. In most realistic computer vision applications, an input image undergoes some form of image distortion such as blur and additive noise during image acquisition or transmission. Deep networks trained on pristine images perform poorly when tested on such distortions. In this paper, we evaluate the effect of image distortions like Gaussian blur and additive noise on the activations of pre-trained convolutional filters. We propose a metric to identify the most noise susceptible convolutional filters and rank them in order of the highest gain in classification accuracy upon correction. In our proposed approach called DeepCorrect, we apply small stacks of convolutional layers with residual connections, at the output of these ranked filters and train them to correct the worst distortion affected filter activations, whilst leaving the rest of the pre-trained filter outputs in the network unchanged. Performance results show that applying DeepCorrect models for common vision tasks like image classification (CIFAR-100, ImageNet), object recognition (Caltech-101, Caltech-256) and scene classification (SUN-397), significantly improves the robustness of DNNs against distorted images and outperforms the alternative approach of network fine-tuning.*

which were previously considered to be extremely difficult, have seen great improvements in their state-of-the-art results due to the use of DNNs. An important factor contributing to the success of such deep architectures in computer vision tasks is the availability of large scale annotated datasets (Deng et al, 2009; Lin et al, 2014).

The visual quality of input images is an aspect very often overlooked while designing DNN based computer vision systems. In most realistic computer vision applications, an input image undergoes some form of image distortion including blur and additive noise during image acquisition, transmission or storage. However, most popular large scale datasets do not have images with such artifacts. Dodge and Karam (2016) showed that even though such image distortions do not represent adversarial samples for a DNN, they do cause a considerable degradation in classification performance. Figure 1 shows the effect of image quality on the prediction performance of a DNN trained on high quality images devoid of distortions.

Testing distorted images with a pre-trained DNN model for AlexNet (Krizhevsky et al, 2012), we observe that adding even a small amount of distortion to the original image results in a misclassification, even though the added distortion does not hinder the human ability to classify the same images (Figure 1). In the cases where the predicted label for a distorted image is correct, the prediction confidence drops significantly as the distortion severity increases.

## 1. Introduction

Today, state-of-the-art algorithms for computer vision tasks like image classification, object recognition and semantic segmentation employ some form of deep neural networks (DNNs). The ease of design for such networks, afforded by numerous open source deep learning libraries (Jia et al, 2014; Chollet, 2015), has established DNNs as the go-to solution for many computer vision applications. Even challenging computer vision tasks like image classification (Simonyan and Zisserman, 2014; Szegedy et al, 2015; He et al, 2016; Krizhevsky et al, 2012) and object recognition (Girshick et al, 2014; Ren et al, 2015; Redmon et al, 2016),

A concise way to observe the impact of image quality on DNN classification performance is to visualize the distribution of classes in the feature space learnt by a DNN. Since DNNs learn high dimensional feature spaces that are difficult to visualize, we use the visualization method proposed by Maaten and Hinton (2008) to embed the high dimensional features from the 4096-dimensional penultimate layer of AlexNet (Krizhevsky et al, 2012), to a 2-dimensional feature space for 11 image classes in the ImageNet dataset. The 11 classes are chosen from the higher levels of the ImageNet WordNet hierarchy, such that no two classes belong to the same node, thus ensuring reasonable

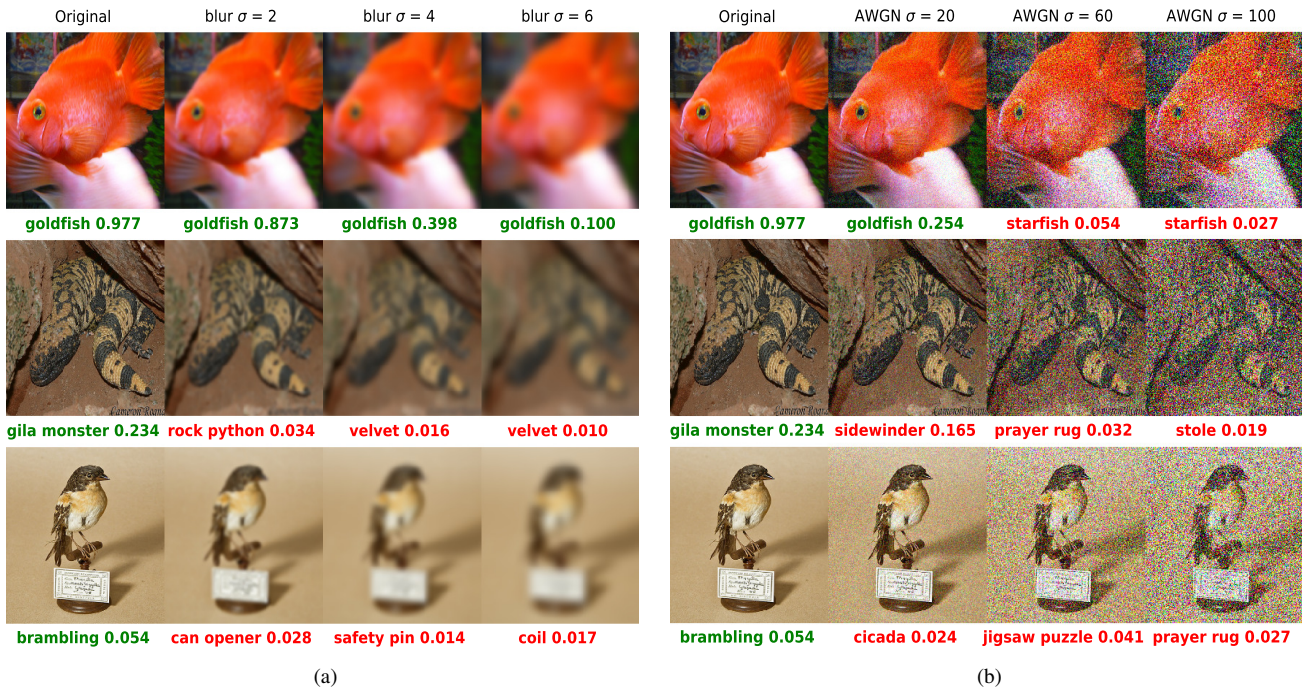


Figure 1. Effect of image quality on DNN predictions, with predicted label and confidence generated by a pre-trained AlexNet (Krizhevsky et al, 2012) model. Distortion severity increases from left to right, with the left-most image in a row having no distortion (original). Green text indicates correct classification, while red denotes misclassification<sup>1</sup>. (a) Examples from the ILSVRC2012 (Deng et al, 2009) validation set distorted by Gaussian blur. (b) Examples from the ILSVRC2012 validation set distorted by Additive White Gaussian Noise (AWGN).

separability of undistorted images of these classes.

Figure 2 shows the effect of image quality on the discriminative power of the features learnt by a DNN from high quality images, through t-SNE embeddings (Maaten and Hinton, 2008) of object classes affected by different types and levels of distortion. One can see that the features of a pre-trained model are discriminative enough to generate a concise clustering of high-quality images from the same class and also provide a good separation between clusters of other classes (Figure 2, column 1). However, the addition of distortion not only reduces the separation between clusters but also causes the clusters to become wider, eventually resulting in most clusters mapping into each other and thus becoming inseparable as the distortion severity increases. This indicates that features learnt from a dataset of high quality images are not invariant to image distortion or noise and cannot be directly used for applications where the quality of images is different than that of the training images. Some issues to consider include the following: For a network trained on undistorted images, are all convolutional filters in the network equally susceptible to noise or blur in the input image? Are networks able to learn some filters that are invariant to input distortions, even when such distortions are absent from the training set? Is it possible

<sup>1</sup>All figures in this paper are best viewed in color.

to identify and rank the convolutional filters that are most susceptible to image distortions and recover the lost performance, by only correcting the outputs of such ranked filters?

In our proposed approach called *DeepCorrect*, we try to address these aforementioned questions by first evaluating the effect of image distortions like Gaussian blur and Additive White Gaussian Noise (AWGN) on the outputs of pre-trained convolutional filters. We observe that for every layer of convolutional filters in the DNN, certain filters are far more susceptible to input distortions than others and that correcting the activations of these filters can help recover lost performance. We then propose a metric to rank the convolutional filters in order of the highest gain in classification accuracy upon correction. Finally, we append *correction units*, which are small blocks of stacked convolutional layers with a single skip connection per block (*residual blocks*), at the output of select filters and train them to correct the worst distortion-affected filter activations using a target-oriented loss, whilst leaving the rest of the pre-trained filter outputs in the network unchanged.

Applying our *DeepCorrect* models for common vision tasks like image classification (Krizhevsky and Hinton (2009), Deng et al (2009)), object recognition (Fei-Fei et al (2007), Griffin et al (2007)) and scene classification (Xiao et al (2010)) significantly improves the robustness of DNNs

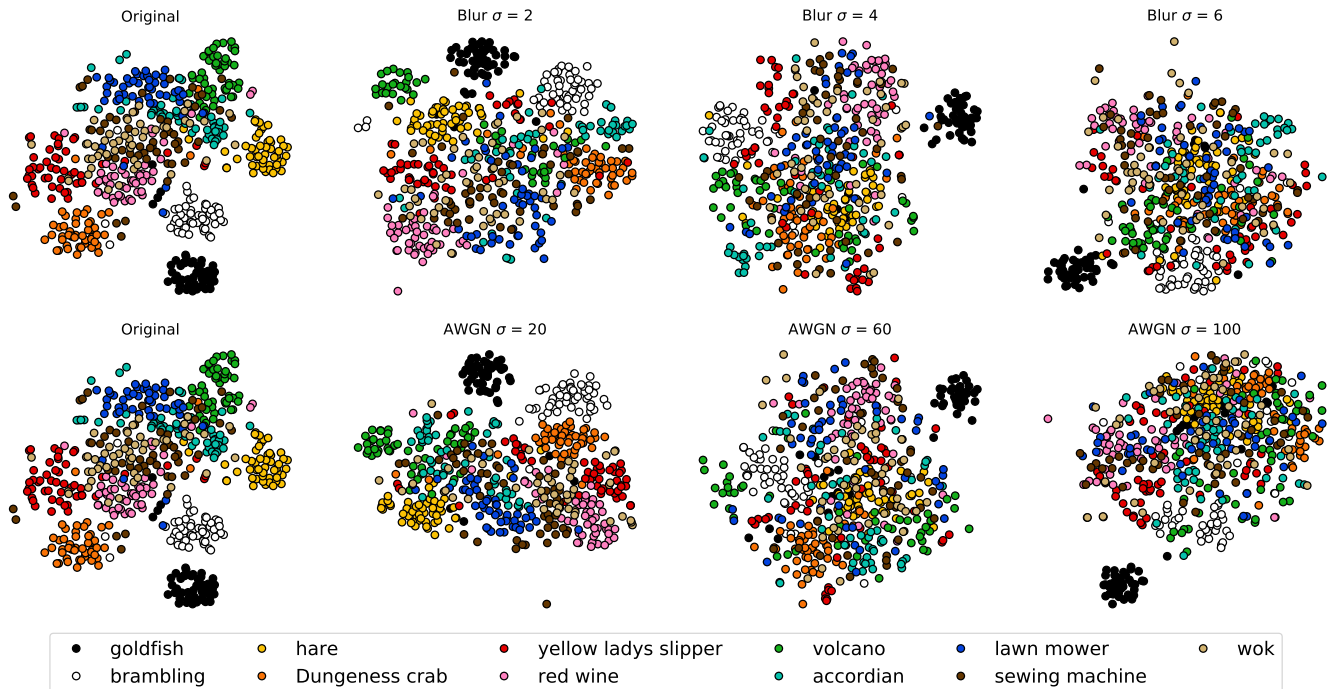


Figure 2. Two-dimensional t-SNE (Maaten and Hinton, 2008) embedding of the penultimate layer features of pre-trained AlexNet, visualized for original (undistorted), blurred and noise affected images of 11 classes from the ILSVRC2012 (Deng et al, 2009) validation set, with each color representing a separate class and distortion severity increasing from left to right. Class labels are chosen from the highest level of the ILSVRC2012 WordNet hierarchy, such that no two classes belong to the same WordNet node, thus ensuring a good segregation between clusters of each class, for clean images. Each point in the embedding represents an image in the 11 class subset, with 50 images per class. **Top row:** Embedding for Gaussian blur affected images. **Bottom row:** Embedding for AWGN affected images.

against distorted images and also outperforms the alternative approach of network fine-tuning, while training significantly lesser parameters than the fine-tuned network.

The remainder of the paper is organized as follows— Section 2 provides an overview of the related work in assessing and improving the robustness of DNNs to input image perturbations. Section 3 describes the distortions, network architectures and datasets we use for analyzing the distortion susceptibility of convolutional filters in a DNN. A detailed description of our proposed approach is presented in Section 4 followed, in Section 5, by extensive tests and experimental validation on multiple datasets covering image classification, object recognition and scene classification. Concluding remarks are given in Section 6.

## 2. Related Work

DNN susceptibility to specific small magnitude perturbations which are imperceptible to humans but cause networks to make erroneous predictions with high confidence (adversarial samples) has been studied by Szegedy et al (2013) and Goodfellow et al (2014). The concept of rubbish samples proposed by Nguyen et al (2015) studies the vulnerability of DNNs to make arbitrary high confidence predictions for random noise images that are completely

unrecognizable to humans, i.e., the images contain random noise and no actual object. However, both adversarial samples and rubbish samples are relatively less encountered in common computer vision applications as compared to other common distortions due to image acquisition, storage, transmission and reproduction.

Lenc and Vedaldi (2015) assess the equivariance and invariance of DNN outputs to affine transformations of the input like scaling, translation and rotation and propose a sparsity based regression solution for learning transformations of DNN outputs to compensate for simple affine transformations of the input.

Karam and Zhu (2015) present QLFW, a face matching dataset consisting of images with five types of quality distortions. Basu et al (2015) present the n-MNIST dataset, which adds Gaussian noise, motion blur and reduced contrast to the original images of the MNIST dataset. Dodge and Karam (2016) evaluate the impact of a variety of quality distortions such as Gaussian blur, AWGN and JPEG compression on various state-of-the-art DNNs and report a substantial drop in classification accuracy on the ImageNet (ILSVRC2012) dataset in the presence of blur and noise. Karahan et al (2016) present a similar evaluation for the task of face recognition.

An obvious approach to improve the resilience of networks trained on high quality images would be to fine-tune the network on images with observed distortion types or in cases where the network size and dataset is not too large, include the image distortion process as a form of data augmentation process and retrain the entire network with such data. [Vasiljevic et al \(2016\)](#) study the effect of various types of blur on the performance of DNNs and show that DNN performance for the task of classification and segmentation drops in the presence of blur. [Vasiljevic et al \(2016\)](#) and [Zhou et al \(2017\)](#) show that fine-tuning a DNN on a dataset comprised of both distorted and undistorted images helps to recover part of the lost performance when the degree of distortion is low.

[Diamond et al \(2017\)](#) propose a joint denoising, deblurring and classification pipeline. This involves an image pre-processing stage that denoises and deblurs the image in a manner that preserves image features optimal for classification rather than aesthetic appearance. The classification stage has to be fine-tuned using distorted and clean images, while the denoising and deblurring stages assume a priori knowledge of camera parameters and the blur kernel which may not be available at the time of testing.

[Rodner et al \(2016\)](#) assess the sensitivity of various DNNs to image distortions like translation, AWGN and salt & pepper noise, for the task of fine grained categorization on the CUB-200-2011 ([Wah et al, 2011](#)) and Oxford flowers ([Nilsback and Zisserman, 2008](#)) datasets, by proposing a first-order Taylor series based gradient approximation that measures the expected change in final layer outputs for small perturbations to input image. Since a gradient approximation assumes small perturbations, Rodner *et al.*'s sensitivity measure does not work well for higher levels of distortion as shown by [Rodner et al](#) and does not assess susceptibility at a filter level within a DNN. Furthermore, Rodner *et al.* do not present a solution for making the network more robust to input distortions; instead, they simply fine-tune the whole network with the distorted images added as part of data augmentation during training. Retraining large networks such as VGG16 ([Simonyan and Zisserman, 2014](#)) or ResNet-50 ([He et al, 2016](#)) on large-scale datasets is computationally expensive. Unlike Rodner *et al.*'s work, our proposed ranking measure assesses sensitivity of individual convolutional filters in a DNN, is not limited to differentiable distortion processes, and holds good for both small and large perturbations.

### 3. Experimental Setup

Here, we describe the various image distortions, datasets and network architectures used to evaluate the susceptibility of individual convolutional filters to input distortions.

#### 3.1. Datasets

We use two popular image classification datasets: 1) CIFAR-100 ([Krizhevsky and Hinton, 2009](#)) which has fixed size images of 32x32 pixels and 2) ImageNet ([Deng et al, 2009](#)) (ILSVRC2012) which has images of varying resolution, usually greater than 128x128 pixels. CIFAR-100 consists of 50000 training images and 10000 testing images covering 100 different object categories. We split the CIFAR-100 training set into two sets: 45000 images for training and 5000 for validation. The ImageNet dataset consists of around 1.3 million training images covering 1000 object classes and 50000 validation images, with 50 validation images per class. We use the validation set of ImageNet for evaluating performance.

#### 3.2. Distortions

We focus on evaluating two important and conflicting types of image distortions: Gaussian blur and AWGN over 6 levels of distortion severity. Gaussian blur, often encountered during image acquisition and compression ([Ponomarenko et al, 2009](#)), represents a distortion that eliminates high frequency discriminative object features like edges and contours, whereas AWGN is commonly used to model additive noise encountered during image acquisition and transmission.

Since we use datasets with different input resolutions, we use a different set of distortion parameters for each dataset. For CIFAR-100, we use a noise standard deviation  $\sigma_n \in \{5, 10, 15, 20, 25, 30\}$  for AWGN and blur standard deviation  $\sigma_b \in \{0.5, 1, 1.5, 2.0, 2.5, 3.0\}$  for Gaussian blur. For ImageNet, a noise standard deviation  $\sigma_n \in \{10, 20, 40, 60, 80, 100\}$  for AWGN and blur standard deviation  $\sigma_b \in \{1, 2, 3, 4, 5, 6\}$  for Gaussian blur, are used. For both datasets, the size of the blur kernel is set to 4 times the blur standard deviation  $\sigma_b$ .

#### 3.3. Network Architectures

Due to the different input resolutions for ImageNet and CIFAR-100 images, we use two different network architectures, specifically: a fully-convolutional network that consists of only convolutional layers with a final 100-way softmax layer for CIFAR-100, and a DNN comprised of both convolutional and fully connected dense layers with a final 1000-way softmax layer for ImageNet. We use the term "pre-trained" or "baseline" network to refer to any network that is trained on undistorted images.

Our version of a fully-convolutional network shown in Figure 3a is based on the All-Convolutional Net proposed by [Springenberg et al \(2014\)](#), with the addition of batch normalization units after each convolutional layer. This network, which serves as our baseline model for CIFAR-100, is trained using stochastic gradient descent and we refer the readers to the work of [Springenberg et al \(2014\)](#) for

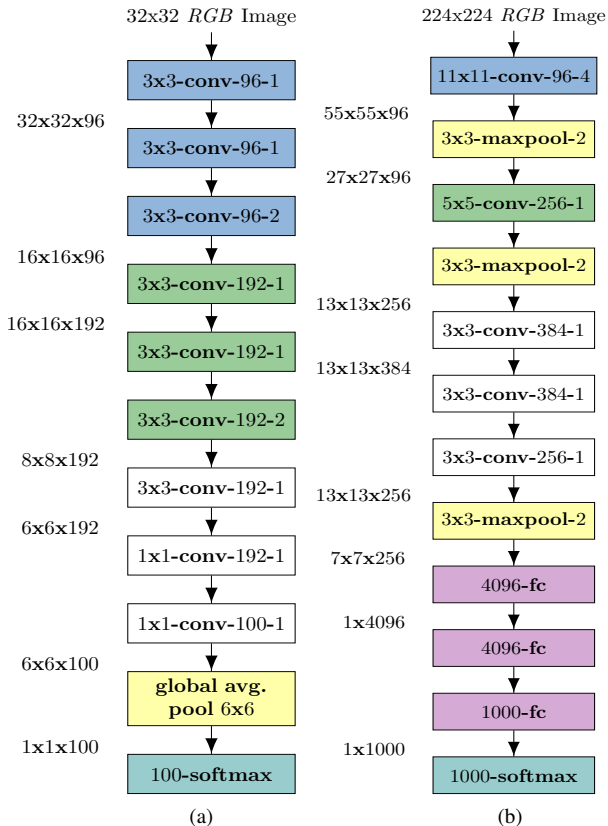


Figure 3. Network architectures for our baseline models. Convolutional layers are parameterized by  $k \times k$ -conv- $d$ - $s$ , where  $k \times k$  is the spatial extent of the filter,  $d$  is the number of output filters in a layer and  $s$  represents the filter stride. Maxpooling layers are parameterized as  $k \times k$ -maxpool- $s$ , where  $s$  is the spatial stride. (a) Fully-convolutional net for CIFAR-100, based on the network architecture proposed by Springenberg et al (2014)<sup>3</sup>. (b) AlexNet DNN for ImageNet proposed by Krizhevsky et al (2012)<sup>4</sup>.

additional details regarding this network architecture and training. The AlexNet DNN proposed by Krizhevsky et al (2012), shown in Figure 3b, is used as our baseline model for the ImageNet dataset<sup>2</sup>.

## 4. DeepCorrect

It is important for a DNN to perform well on both clean and distortion-affected images and an ideal performance curve should have the same accuracy for all levels of distortion severity. Top-1 accuracy for both ImageNet and

<sup>2</sup>We use the code and weights for the AlexNet DNN available online at <https://github.com/heuritech/convnets-keras>

<sup>3</sup>Every convolutional layer is followed by a batch normalization operation and ReLU non-linearity for the CIFAR-100 model.

<sup>4</sup>Every convolutional layer is followed by a ReLU non-linearity for the AlexNet DNN. In addition to the ReLU non-linearity, the first and second convolutional layers of the AlexNet DNN are also followed by a local response normalization operation (Krizhevsky et al, 2012).

CIFAR-100 baseline models is tabulated in Tables 1 and 2. From Tables 1 and 2, it is clear that the networks trained on clean images perform poorly when presented with input images that are distorted even at low distortion levels.

This section describes the main contributions of the paper: 1) measuring the susceptibility of convolutional filters to input distortion using a proposed objective metric and ranking said filters in the order of highest susceptibility to input distortion (Section 4.1), 2) training small *residual blocks*, which we refer to as *correction units*, at the output of these ranked filters to correct their activations against input distortion using a target-oriented loss (Section 4.2).

### 4.1. Ranking Filters through Correction Priority

Although pre-trained networks perform poorly on test images with significantly different image statistics than those used to train these networks (Tables 1 and 2), it is not obvious if only some convolutional filters in a network layer are responsible for most of the observed performance gap or if all convolutional filters in a layer contribute more or less equally to the performance degradation. If only a subset of the filters in a layer are responsible for most of the lost performance, we can avoid modifying all the remaining filter activations in a DNN. By focusing on restoring the activations of only select filters which are most susceptible to input distortions, we can reduce the time and computational resources involved in enhancing DNN robustness to distortions.

We define the output of a single convolutional filter  $\phi_{i,j}$  to the input  $\mathbf{x}_i$  by  $\phi_{i,j}(\mathbf{x}_i)$ , where  $i$  and  $j$  correspond to layer number and filter number, respectively. If  $g_i(\cdot)$  is a transformation that models the distortion acting on filter input  $\mathbf{x}_i$ , then the output of a convolutional filter  $\phi_{i,j}$  to the distortion affected input is given by  $\widetilde{\phi}_{i,j}(\mathbf{x}_i) = \phi_{i,j}(g_i(\mathbf{x}_i))$ . It should be noted that  $\widetilde{\phi}_{i,j}(\mathbf{x}_i)$  represents the filter activations generated by distorted inputs and  $\phi_{i,j}(\mathbf{x}_i)$  represents the filter activations for undistorted inputs. Assuming we have access to  $\phi_{i,j}(\mathbf{x}_i)$  for a given set of input images, replacing  $\widetilde{\phi}_{i,j}(\mathbf{x}_i)$  with  $\phi_{i,j}(\mathbf{x}_i)$  in a deep network is akin to perfectly correcting the activations of the convolutional filter  $\phi_{i,j}$  against input image distortions. Computing the output predictions by swapping a distortion affected filter output with its corresponding clean output for each of the ranked filters would improve classification performance. The extent of improvement in performance is indicative of the susceptibility of a particular convolutional filter to input distortion and its contribution to the associated performance degradation.

We now define the correction priority of a convolutional filter  $\phi_{i,j}$  as the improvement in DNN performance on a validation set, generated by replacing  $\widetilde{\phi}_{i,j}(\mathbf{x}_i)$  with  $\phi_{i,j}(\mathbf{x}_i)$  for a pre-trained network. Let the baseline performance (computed over distorted images) for a network be  $p_b$ , which

Table 1. Top-1 accuracy of pre-trained networks for Gaussian blur affected images. The severity of distortion increases from Level 1 to 6, where 1 is the least severe and 6 is the most severe, while clean represents undistorted images. ImageNet :  $\sigma_b \in \{1, 2, 3, 4, 5, 6\}$ , CIFAR-100 :  $\sigma_b \in \{0.5, 1, 1.5, 2.0, 2.5, 3.0\}$ .

Dataset	Distortion Level							Avg
	Clean	Level 1	Level 2	Level 3	Level 4	Level 5	Level 6	
ImageNet	0.5694	0.4456	0.2934	0.1585	0.0786	0.0427	0.0256	0.2305
CIFAR-100	0.7028	0.6402	0.2212	0.0806	0.0440	0.0340	0.0290	0.2502

Table 2. Top-1 accuracy of pre-trained networks for images distorted by additive white Gaussian noise. The severity of distortion increases from Level 1 to 6, where 1 is the least severe and 6 is the most severe, while clean represents undistorted images. ImageNet :  $\sigma_n \in \{10, 20, 40, 60, 80, 100\}$ , CIFAR-100 :  $\sigma_n \in \{5, 10, 15, 20, 25, 30\}$ .

Dataset	Distortion Level							Avg
	Clean	Level 1	Level 2	Level 3	Level 4	Level 5	Level 6	
ImageNet	0.5694	0.5218	0.3742	0.1256	0.0438	0.0190	0.0090	0.2375
CIFAR-100	0.7028	0.6184	0.3862	0.2239	0.1324	0.0829	0.0569	0.3147

can be obtained by computing the average top-1 accuracy of the network over a set of images or another task-specific performance measure. Let  $p_{swp}(i, j)$  denote the new improved performance of the network after swapping  $\widetilde{\phi}_{i,j}(\mathbf{x}_i)$  with  $\phi_{i,j}(\mathbf{x}_i)$ . As our implementation focuses on classification tasks, the average top-1 accuracy over a set of distorted images is used to measure  $p_b$  and  $p_{swp}(i, j)$ . The correction priority for filter  $\phi_{i,j}$  is then given by:

$$\tau(i, j) = p_{swp}(i, j) - p_b \quad (1)$$

The higher the value of  $\tau(i, j)$ , the more susceptible the convolutional filter  $\phi_{i,j}$  is to input distortion. For computing the correction priorities, we form two small validation subsets, one that contains 1000 images (i.e, 10 images per class) randomly sampled from the CIFAR-100 validation set for computing correction priorities for the CIFAR-100 DNN, and another one consisting of 5000 images (i.e, 5 images per class) randomly sampled from the ImageNet training set for computing correction priorities for the AlexNet DNN.

Using the proposed ranking measure in Equation (1), we compute correction priorities for every convolutional filter in the network and rank the filters in descending order of correction priority. The detailed overview and pseudo-code for computing correction priorities is summarized in Algorithm 1. The correction priority for convolutional filters can be used to rank filters locally (i.e, rank only the filters within a layer) as well as globally (i.e, rank the filters across layers). We evaluate the impact of both a local ranking scheme and a global ranking scheme on DNN robustness to distortions in Section 5.1 and Section 5.2.

We evaluate in Figure 4, the effect of correcting different percentages of the ranked filter activations ( $\beta_i$ ) in the  $i^{th}$  DNN layer. For the CIFAR-100 model, it is possible to recover a large part of the lost performance for both Gaussian blur and AWGN respectively, by correcting only 25% of the

filter activations in the first layer. However for AlexNet, the number of filter activations in the first layer that need correction is higher. An interesting observation in Figure 4 is the relatively higher improvement in accuracy going from 50% to 75% corrected filter activations for ImageNet images affected by Gaussian blur. This can be attributed to at least some, if not most of the top 50% ranked filters being highly correlated. While ranking and choosing a subset of filters to correct, we assumed that each filter’s contribution to the final prediction accuracy is independent of the remaining filters in a layer. However in many cases, there may be high correlation between filters of a layer and the number of filters to be corrected can be further reduced by identifying the highly susceptible uncorrelated filters. Identifying the smallest set of uncorrelated distortion susceptible filters that maximize robustness to input distortion upon correction, would be the subject of our future work.

Figure 5 summarizes the performance of different layers of a network, obtained after correcting 50% filter outputs in the respective layer of CIFAR-100 DNN and 75% filter outputs in the respective layer of AlexNet. For both CIFAR-100 and ImageNet models, the best performance is achieved by correcting filter activations in the early convolutional layers (i.e, conv-1 for CIFAR-100 model and conv-2 for AlexNet) and as we go deeper in the network, accuracy diminishes for correcting a fixed percentage of filter outputs. This indicates that, as we go deeper in the network, all the convolutional filters become more or less equally susceptible to distortion.

Convolutional filter visualizations from the first layer of the pre-trained AlexNet model (Figure 6a) reveal two types of filter kernels: 1) mostly color agnostic, frequency- and orientation-selective filters that capture edges and object contours and 2) color specific blob shaped filters that are sensitive to specific color combinations. Figs. 6b and 6c, visualize the top 50% filters in the first convolutional layer

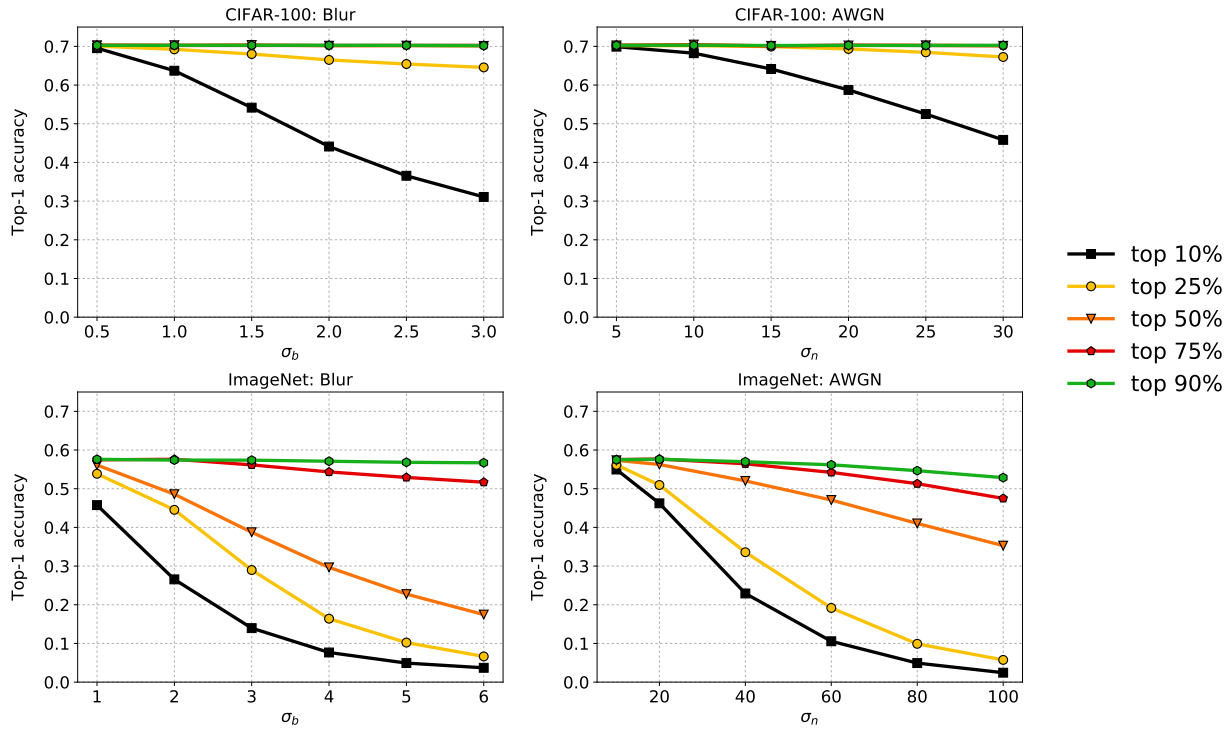


Figure 4. Effect of varying the percentage of corrected filter activations  $\beta_1 \in \{10\%, 25\%, 50\%, 75\%, 90\%\}$ , in the first convolutional layer (conv-1) of pre-trained networks, for both Gaussian blur affected images and AWGN affected input images.

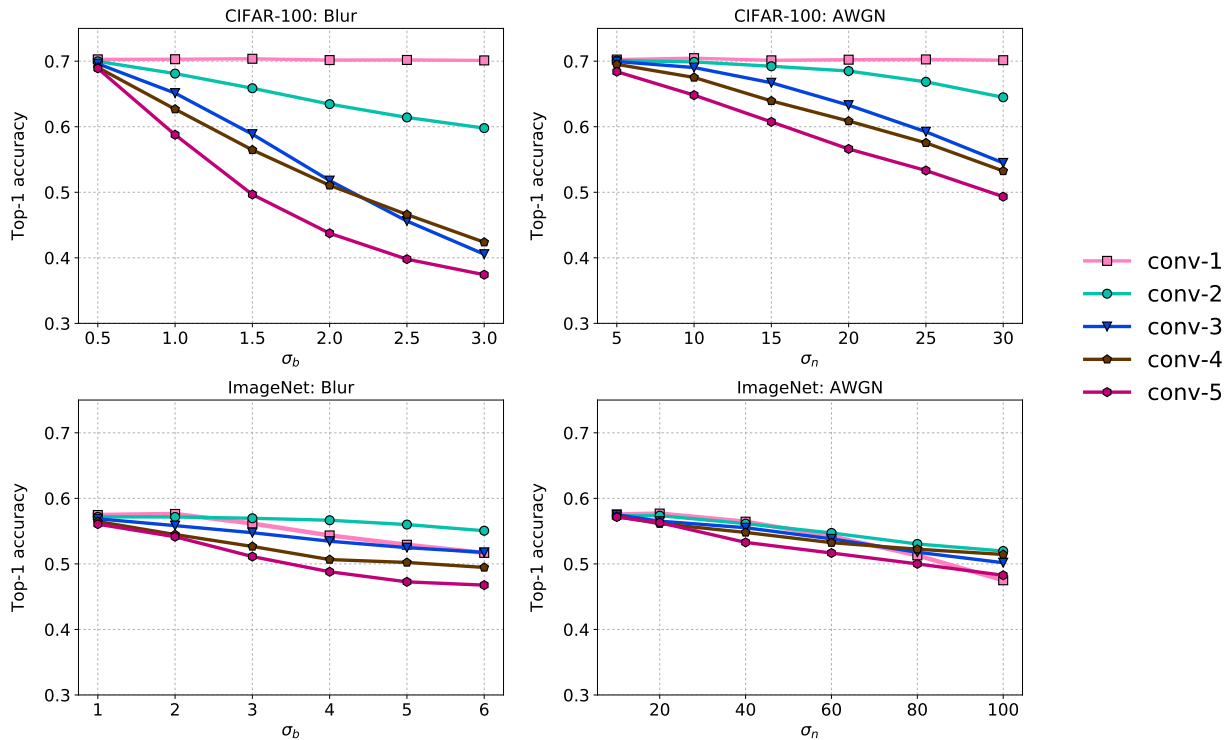


Figure 5. Effect of correcting  $\beta_i N_i$  filter activations in a single convolutional layer in a network, for images affected by Gaussian Blur and images affected by AWGN, where conv- $i$  represents the corrected  $i^{\text{th}}$  convolutional layer in a network and  $N_i$  represents the number of convolutional filters in the  $i^{\text{th}}$  layer. For CIFAR-100 DNN,  $\beta_i = 50\%$  with  $1 \leq i \leq 5$ . For ImageNet DNN (AlexNet),  $\beta_i = 75\%$  with  $1 \leq i \leq 5$ .

---

**Algorithm 1: Computing Correction Priority**

---

Given input triplets

$(\mathbf{x}_{1,i}, g_i(\mathbf{x}_{1,i}), y_1), \dots, (\mathbf{x}_{M,i}, g_i(\mathbf{x}_{M,i}), y_M)$  with  $1 \leq i \leq L$ , where  $i$  represents the layer number,  $\mathbf{x}_{m,i}$  is the  $m^{\text{th}}$  undistorted input for layer  $i$  and  $g_i(\mathbf{x}_{m,i})$  is the corresponding distorted version,  $M$  is the total number of images in the validation set and  $y_m$  is the ground-truth label for the  $m^{\text{th}}$  input image.

$p_b = 0$

**for**  $m = 1$  to  $M$  **do**

    predict class label  $y_{pred_m}$  for distorted input image  $g_1(\mathbf{x}_{m,1})$

$p_b = p_b + \frac{1}{M}h(y_m, y_{pred_m})$

    where  $h(y_m, y_{pred_m}) = 1$ , if  $y_m = y_{pred_m}$  and 0 otherwise.

**end**

**for**  $i = 1$  to  $L$  **do**

$N_i$ : number of filters in layer  $i$

$\phi_{i,j}$  is a convolutional filter, where  $j$  is the filter number and  $i$  is the layer number

**for**  $j = 1$  to  $N_i$  **do**

$p_{swp}(j) = 0$

**for**  $m = 1$  to  $M$  **do**

            swap distorted filter output with clean

            output,  $\phi_{i,j}(g_i(\mathbf{x}_{m,i})) \leftarrow \phi_{i,j}(\mathbf{x}_{m,i})$

            predict class label  $y_{pred_m}$

$p_{swp}(j) = p_{swp}(j) + \frac{1}{M}h(y_m, y_{pred_m})$

            where  $h(y_m, y_{pred_m}) = 1$ , if  $y_m = y_{pred_m}$  and 0 otherwise.

**end**

$\tau(i, j) = p_{swp}(j) - p_b$

**end**

**end**

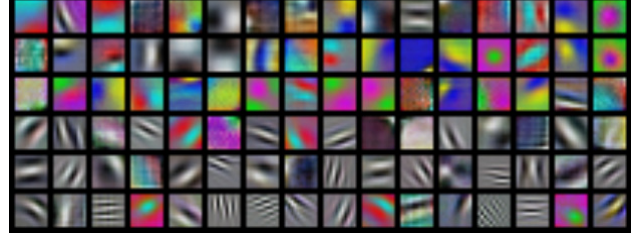
---

of AlexNet, that are most susceptible to Gaussian blur and AWGN, respectively, as identified by our proposed ranking metric. The identified filters most susceptible to Gaussian blur are mainly frequency- and orientation-selective filters, most of which are color agnostic, while filters most susceptible to AWGN are a mix of both color specific blobs and frequency- and orientation-selective filters. This is in line with our intuitive understanding that Gaussian blur majorly affects edges and object contours and not object color, while AWGN affects color as well as object contours.

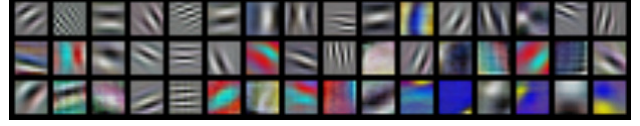
## 4.2. Correcting Ranked Filter Outputs

Here, we propose a novel approach, which we refer to as *DeepCorrect*, where we learn a task-driven corrective transform that acts as a distortion masker for convolutional filters that are most susceptible to input distortion, while leav-

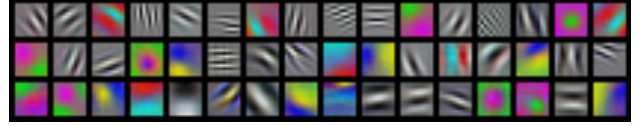
<sup>5</sup>Color contrast for visualizations has been enhanced to improve readability.



(a)



(b)



(c)

Figure 6. (a) 96 convolutional filter kernels of size  $11 \times 11 \times 3$  in the first convolutional layer of pre-trained AlexNet<sup>5</sup>. (b) Convolutional filter kernels most susceptible to Gaussian blur (top 50%), as identified by our proposed ranking metric. (c) Convolutional filter kernels most susceptible to AWGN (top 50%), as identified by our proposed ranking metric. In (b) and (c), the filters are sorted in descending order of susceptibility going row-wise from top left to bottom right.

ing all the other pre-trained filter outputs in the layer unchanged. Let  $R_i$  represent a set consisting of the  $N_i$  ranked filter indices in the  $i^{\text{th}}$  layer of the network, computed using the procedure in Section 4.1. Also let  $R_{i,\beta_i}$  represent a subset of  $R_i$  consisting of the top  $\beta_i N_i$  ranked filter indices in network layer  $i$ , where  $N_i$  is the total number of convolutional filters in layer  $i$  and  $\beta_i$  is the percentage of filters corrected in layer  $i$ , as defined in Section 4.1. If  $\Phi_i$  represents the set of convolutional filters in the  $i^{\text{th}}$  layer, the objective is to learn a transform  $F_{corr_i}(\cdot)$  such that:

$$F_{corr_i}(\Phi_{R_{i,\beta_i}}(g_i(\mathbf{x}_i))) \approx \Phi_{R_{i,\beta_i}}(\mathbf{x}_i) \quad (2)$$

where  $\mathbf{x}_i$  is the undistorted input to the  $i^{\text{th}}$  layer of convolutional filters and  $g_i(\cdot)$  is a transformation that models the distortion acting on  $\mathbf{x}_i$ . Since we do not assume any specific form for the image distortion process, we let the corrective transform  $F_{corr_i}(\cdot)$  take the form of a shallow *residual block*, which is a small stack of convolutional layers (4 layers) with a single skip connection (He et al, 2016), such as the one shown in Figure 7. We refer to such a *residual block* as a *correction unit*.  $F_{corr_i}(\cdot)$  can now be estimated using a target-oriented loss such as the one used to train the original network, through backpropagation (Rumelhart et al, 1995), but with much less number of parameters.

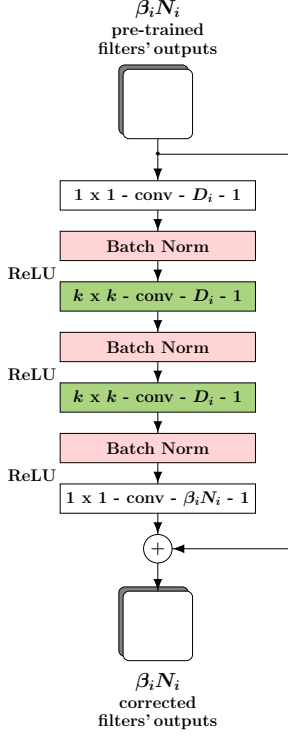


Figure 7. *Correction unit* based on a residual function (He et al, 2016), acting on the outputs of  $\beta_i N_i$  ( $0 < \beta_i < 1$ ) filters out of  $N_i$  total filters in the  $i^{th}$  convolutional layer of a pre-trained DNN. All convolutional layers in the *residual block*, except the first and last layer, are parameterized by  $k \times k$ -conv- $D_i$ - $s$ , where  $k \times k$  is spatial extent of the filter,  $D_i$  (correction width) is the number of output filters in a layer,  $s$  represents the filter stride and  $i$  represents the layer number of the convolutional layer being corrected in the pre-trained DNN.

Consider an  $L$  layered DNN  $\Phi$  that has been pre-trained for an image classification task using clean images.  $\Phi$  can be interpreted as a function that maps network input  $\mathbf{x}$  to an output vector  $\Phi(\mathbf{x}) \in \mathbb{R}^d$ , such that:

$$\Phi = \Phi_L \circ \Phi_{L-1} \circ \dots \circ \Phi_2 \circ \Phi_1 \quad (3)$$

where  $\Phi_i$  is the mapping function (set of convolutional filters) representing the  $i^{th}$  DNN layer and  $d$  is the dimensionality of the network output.

Without loss of generality, if we add a *correction unit* that acts on the top  $\beta_1 N_1$  ranked filters in the first network layer, then the resultant network  $\Phi_{corr}$  is given by:

$$\Phi_{corr} = \Phi_L \circ \Phi_{L-1} \circ \dots \circ \Phi_2 \circ \Phi_{1_{corr}} \quad (4)$$

<sup>6</sup>The *correction unit* is applied before the batch normalization operation and ReLU non-linearity acting upon the distortion-susceptible convolutional filter outputs.

<sup>7</sup>The *correction unit* is applied before the ReLU non-linearity acting upon the distortion-susceptible convolutional filter outputs. Max pooling layers following convolutional layers 1, 2 and 5 in the pre-trained AlexNet have not been shown in the ImageNet Deepcorr-5 model for uniformity.

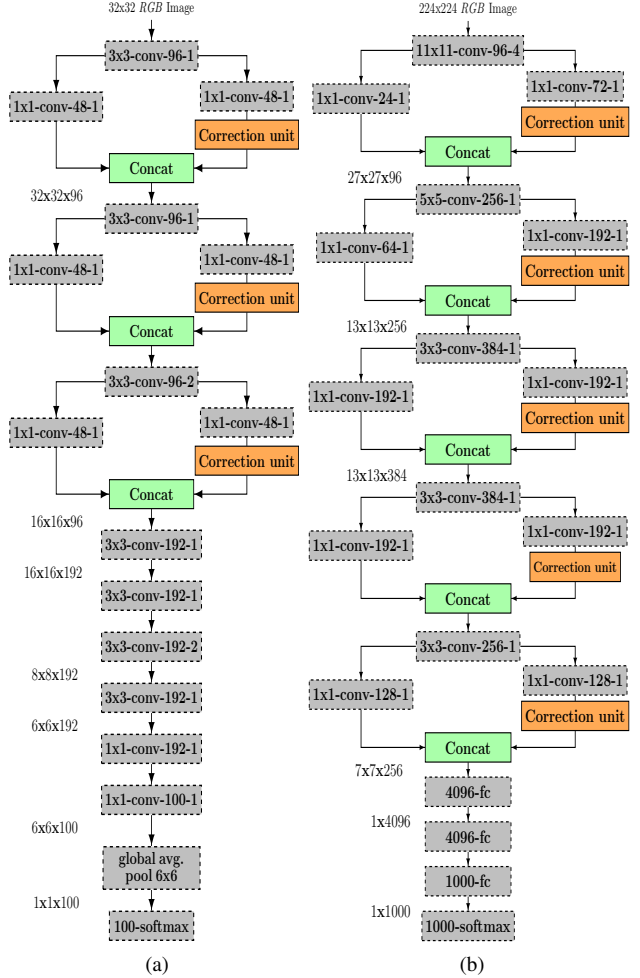


Figure 8. Examples of *DeepCorrect* models for CIFAR-100 and ImageNet datasets. Convolution layers from the original architectures in Figure 3, shown in gray with dashed outlines, are non-trainable layers and their weights are kept the same as those of the pre-trained model. (a) Deepcorr-3 for CIFAR-100, with 50% filter outputs corrected in the first 3 layers<sup>6</sup>. (b) Deepcorr-5 model for ImageNet, with 75% filter outputs corrected in the first two layers and 50% filter outputs corrected in the next three layers<sup>7</sup>.

where  $\Phi_{1_{corr}}$  represents the new mapping function for the first layer, in which the corrective transform  $F_{corr_1}(\cdot)$  acts on the activations of the filter subset  $\Phi_{R_1, \beta_1}$  and all the remaining filter activations are left unchanged. If  $\mathbf{W}_1$  represents the trainable parameters in  $F_{corr_1}$ , then  $F_{corr_1}$  can be estimated by minimizing :

$$E(\mathbf{W}_1) = \lambda \mathcal{R}(\mathbf{W}_1) + \frac{1}{M} \sum_{m=1}^M \mathcal{L}(y_m, \Phi_{corr}(\mathbf{x}_m)) \quad (5)$$

where  $\lambda$  is a constant,  $\mathcal{R}$  is a regularizer such as  $l_1$  norm or  $l_2$  norm,  $\mathcal{L}$  is a standard cross-entropy classification loss,  $y_m$  is the target output label for the  $m^{th}$  input image  $\mathbf{x}_m$ ,  $M$

represents the total number of images in the training set and since we train on a collection of both distorted and clean images,  $\mathbf{x}_m$  represents a clean or a distorted image. The trainable parameters in Equation (5) are  $\mathbf{W}_1$ , while all other network parameters are fixed and kept the same as those in the pre-trained models. Although Equation (5) shows *correction unit* estimation for only the first layer, it is possible to add such units at the output of distortion susceptible filters in any layer and in one or more layers. Figure 8 shows examples of *DeepCorrect* models for the pre-trained networks in Figure 3.

## 5. Experimental Results

We evaluate the proposed approach and the most obvious alternative of fine-tuning baseline models to distortion affected distributions on the two datasets and architectures mentioned in Section 3. The DNN models are trained and tested using the python-based deep learning framework Keras (Chollet, 2015) and a single Nvidia Titan-X GPU. The classification performance is evaluated independently for each type of distortion. Although we report the classification accuracy for each distortion level separately, for both our method and fine-tuning, a single model that can be used to classify images affected by different levels of distortion including the undistorted images is learnt. Unlike common image denoising and deblurring methods like BM3D (Dabov et al, 2009) and NCSR (Dong et al, 2013) which expect the distortion/noise severity to be known or learning-based methods that train separate models for each noise/distortion severity, our *DeepCorrect* based models are totally blind to the severity of distortion added to a test image.

### 5.1. CIFAR-100 Analysis

#### 5.1.1 Fine-tuned models

We fine-tune the CIFAR-100 pre-trained model shown in Figure 3a on a mix of distortion affected images and clean images. Similar to the procedure followed by Vasiljevic et al (2016), we use a mini-batch size of 250 samples, such that half of the input samples in each mini-batch are randomly chosen and distorted with a distortion level that is also chosen randomly. Starting with an initial learning rate that is 10 times lower than the initial learning rate used to generate the pre-trained model, i.e., 0.01, and momentum equal to 0.9, network parameters in various layers are updated for a fixed number of iterations (40 epochs), with the learning rate reduced by a factor of 10 after every 10 epochs. We use a data augmentation method similar to He et al (2016).

We evaluate in Tables 3 and 4, the effect of varying the number of layers that are fine-tuned in a pre-trained network by generating numerous fine-tuned models which are

parameterized by Finetune- $k$ , where  $k$  represents the number of convolutional layers that are fine-tuned, starting from the input. The rest of the layers are left unchanged from a pre-trained model. For Gaussian blur affected images, fine-tuning parameters in all layers (Finetune-9) achieves the highest accuracy among all fine-tuned models, whereas Finetune-6, Finetune-3 and Finetune-1 can achieve  $\approx 98\%$ ,  $87\%$  and  $60\%$  of this accuracy. A similar trend is seen for AWGN and this implies that fine-tuning just a few layers in a DNN is insufficient to make a network robust to distortion.

#### 5.1.2 DeepCorrect models

Similar to the Finetune- $k$  model variants, we can generate numerous *DeepCorrect* models by varying the number of network layers to be corrected, starting from the input, and by applying in these layers, *correction units* (Figure 7) at the output of the ranked distortion susceptible filters of our pre-trained model (Figure 3a); as discussed in Section 4.1, these filters are identified based on the correction priority computed using Algorithm 1. We formulate parameterized *DeepCorrect* models given by Deepcorr- $k$ , where  $k$  represents the number of corrected convolutional layers, starting from the first convolutional layer with  $1 \leq k \leq 6$ . In each corrected layer, the activations of only  $\beta_i N_i$  filters are corrected while leaving all remaining filters' activations unchanged, with  $\beta_i$  being the percentage of filter activations corrected and  $N_i$  being the total number of convolutional filters in DNN layer  $i$ . For example, Figure 8a shows Deepcorr-3. The value for  $\beta_i$  is chosen to be 0.5, i.e., 50% filter activations are corrected per layer. The correction priority computed using Algorithm 1 is used to independently rank the distortion susceptible filters within each layer (local ranking) and correct the activations of the top 50% filters in each layer. For each one of the Deepcorr- $k$  models, we also generate a corresponding model named Deepcorr- $kc$ , where all parameters in the last 3 convolutional layers are also updated in addition to the trainable parameters of the respective Deepcorr- $k$  model. All *DeepCorrect* models are trained as described in Section 4.2, using an initial learning rate of 0.1 and the same learning rate schedule, data augmentation and total iterations used for generating the fine-tuned models.

As shown in Tables 3 and 4, Deepcorr-1, Deepcorr-3 and Deepcorr-6 consistently outperform their fine-tuned model counterparts, i.e., Finetune-1, Finetune-3 and Finetune-6, for both Gaussian blur and AWGN. For Gaussian blur, Deepcorr-1, Deepcorr-3 and Deepcorr-6 achieve  $\approx 46\%$ ,  $16\%$  and  $6\%$  improvement in average accuracy relative to Finetune-1, Finetune-3 and Finetune-6, respectively, while for AWGN the relative improvement in respective average accuracy is  $\approx 14\%$ ,  $3\%$  and  $1\%$ .

Finally in Table 5, we evaluate the effect of using a

Table 3. Top-1 accuracy of various models for Gaussian blur affected images of the CIFAR-100 test set. Bold numbers show best accuracy and underlined numbers show next best accuracy for each distortion level.

Method	Distortion Level							Avg	# Params
	$\sigma_b = 0$	$\sigma_b = 0.5$	$\sigma_b = 1$	$\sigma_b = 1.5$	$\sigma_b = 2.0$	$\sigma_b = 2.5$	$\sigma_b = 3$		
Baseline	<b>0.7028</b>	0.6402	0.2212	0.0806	0.0440	0.0340	0.0290	0.2502	1,389,804
Finetune-1	0.6310	0.6254	0.4664	0.2824	0.1694	0.1139	0.0761	0.3378	2,880
Finetune-3	0.6642	0.6573	0.5905	0.5169	0.4291	0.3431	0.2678	0.4955	169,344
Finetune-6	0.6887	0.6841	0.6266	0.5702	0.5088	0.4544	0.3931	0.5608	1,000,512
Finetune-9	0.6875	0.6808	0.6296	0.5789	0.5297	0.4812	0.4218	0.5727	1,389,804
Deepcorr-1	0.6746	0.6500	0.5787	0.5217	0.4307	0.3395	0.2466	0.4917	80,954
Deepcorr-3	0.6890	0.6781	0.6414	0.5944	0.5441	0.4769	0.4007	0.5749	242,862
Deepcorr-6	<u>0.6963</u>	<u>0.6871</u>	<u>0.6548</u>	<u>0.6116</u>	<u>0.5638</u>	<u>0.5128</u>	0.4405	<u>0.5952</u>	505,674
Deepcorr-1c	0.6893	0.6806	0.6344	0.5905	0.5253	0.4643	0.3961	0.5686	470,246
Deepcorr-3c	0.6947	<u>0.6871</u>	0.6515	0.6035	0.5617	0.5086	<u>0.4456</u>	0.5932	632,154
Deepcorr-6c	0.6937	<b>0.6874</b>	<b>0.6552</b>	<b>0.6118</b>	<b>0.5720</b>	<b>0.5269</b>	<b>0.4694</b>	<b>0.6023</b>	894,966

Table 4. Top-1 accuracy of various models for AWGN affected images of the CIFAR-100 test set. Bold numbers show best accuracy and underlined numbers show next best accuracy for each distortion level.

Method	Distortion Level							Avg	# Params
	$\sigma_n = 0$	$\sigma_n = 5$	$\sigma_n = 10$	$\sigma_n = 15$	$\sigma_n = 20$	$\sigma_n = 25$	$\sigma_n = 30$		
Baseline	<b>0.7028</b>	0.6184	0.3862	0.2239	0.1324	0.0829	0.0569	0.3147	1,389,804
Finetune-1	0.6358	0.6391	0.6257	0.5859	0.5213	0.4571	0.3760	0.5487	2,880
Finetune-3	0.6832	0.6771	0.6588	0.6329	0.6070	0.5694	0.5220	0.6214	169,344
Finetune-6	0.6843	0.6845	0.6687	0.6465	0.6245	0.5940	0.5593	0.6374	1,000,512
Finetune-9	0.6876	0.6838	0.6719	<b>0.6562</b>	<b>0.6317</b>	<b>0.6104</b>	<u>0.5742</u>	<u>0.6451</u>	1,389,804
Deepcorr-1	0.6930	0.6802	0.6612	0.6339	0.6030	0.5688	0.5330	0.6247	80,954
Deepcorr-3	0.6932	0.6846	0.6732	0.6436	0.6181	0.5914	0.5604	0.6377	242,862
Deepcorr-6	<u>0.6964</u>	<b>0.6903</b>	<u>0.6769</u>	0.6496	0.6277	0.5986	0.5679	0.6439	505,674
Deepcorr-1c	0.6952	0.6864	0.6715	0.6467	0.6260	0.5985	0.5642	0.6412	470,246
Deepcorr-3c	<u>0.6964</u>	<u>0.6893</u>	<b>0.6776</b>	<u>0.6512</u>	0.6290	0.6010	0.5723	<b>0.6452</b>	632,154
Deepcorr-6c	0.6930	0.6879	0.6727	0.6484	<u>0.6304</u>	<u>0.6084</u>	<b>0.5757</b>	<b>0.6452</b>	894,966

Table 5. Top-1 accuracy of the Deepcorr-6c model for the CIFAR-100 test set, with filter outputs for correction chosen using either a local or global ranking approach. Performance is reported in terms of Top-1 accuracy averaged over all distortion levels, including original images.

Filter ranking	Gaussian blur	AWGN
Local	0.6023	0.6452
	# corrected per layer	# corrected per layer
	{48, 48, 48, 96, 96, 96}	{48, 48, 48, 96, 96, 96}
Global	0.6025	0.6467
	# corrected per layer	# corrected per layer
	{33, 46, 75, 95, 90, 93}	{30, 44, 61, 103, 99, 95}

global ranking approach for Deepcorr-6c, where we use the correction priority computed using Algorithm 1 to rank fil-

ters across all six convolutional layers and identify the top 50% distortion susceptible filters among them. By correcting the same number of total filter activations as the local ranking approach (432 filters out of 864), we observe that the global ranking approach marginally outperforms the local ranking approach. A paired sample t-test between the local and global ranking accuracies yielded a p-value of 0.2151 ( $> 0.05$ ), i.e., the difference between the global and local ranking accuracies was not statistically significant.

### 5.1.3 Correcting ranked filters vs. random filters

We assess the impact of our ranking metric proposed in Section 4.1, on the performance of our Deepcorr-1 model by training *correction units* on: 1)  $\beta_1 N_1$  filters most susceptible to distortion, as identified by our ranking metric and 2) random subset of  $\beta_1 N_1$  convolutional filters, where  $\beta_1$  and  $N_1$ , as defined in Section 4.1, represent the percentage of filters corrected in the first layer and the total number of

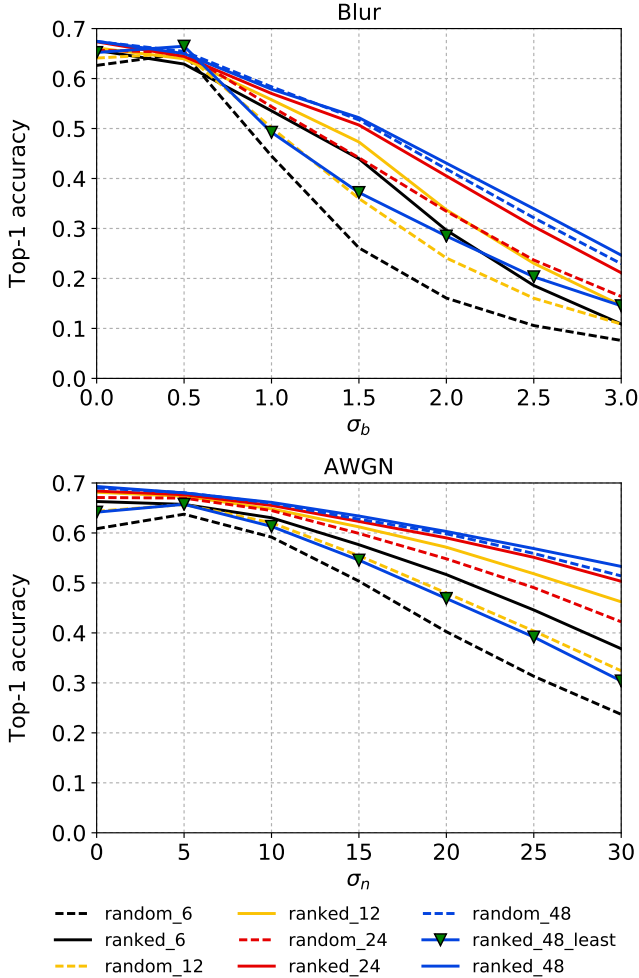


Figure 9. Correcting ranked filter outputs vs. randomly chosen filter outputs, in the first convolutional layer of the CIFAR-100 model. Models correcting the most susceptible ranked filter outputs are represented by ranked. $l$  (solid line) and models correcting a randomly chosen set of filter outputs are represented by random. $l$  (dashed line), where  $l$  is the number of corrected filters. Model correcting the 48 least distortion susceptible filters’ outputs is represented by ranked\_48\_least. **Top:** Top-1 accuracy for Gaussian blur affected images. **Bottom:** Top-1 accuracy for AWGN affected images.

filters in the first layer, respectively. For this analysis, we evaluate DNN accuracy for correcting 6, 12, 24, and 48 filters out of the 96 filters in the first convolutional layer, i.e.  $\beta_1 \in \{6.25\%, 12.5\%, 25\%, 50\%\}$ .

Figure 9 shows the impact of the proposed ranking metric on the performance of Deepcorr-1 for varying number of corrected filters ( $\beta_1 N_1$ ), with models correcting ranked filter outputs represented by ranked. $l$  (solid line) and models correcting a randomly chosen set of filter outputs represented by random. $l$  (dashed line), where  $l$  is the number of corrected filters. We perform 10 trials for choosing different random subsets of filter outputs to be corrected and

Table 6. P-values for paired sample t-test between the ranked. $l$  and random. $l$  models for  $l \in \{6, 12, 24, 48\}$ .

6 filters	12 filters	24 filters	48 filters
0.0001	0.00014	0.0002	0.0119

report in Figure 9, the accuracy averaged over 10 trials, for each level of distortion and type. For a fixed number of corrected filter outputs, adding *correction units* at the output of ranked distortion susceptible filters achieves higher accuracy as compared to adding *correction units* at the output of randomly chosen filters in a convolutional layer.

Interestingly, we observe that in each of the 10 trails for the random\_48 model, at least some of the filters chosen for correction are also present in the set of the 48 most distortion susceptible filters (50%) identified by our proposed ranking measure. For the case where 50% filter outputs are corrected in Deepcorr-1, if the superior performance of our *DeepCorrect* model is only due to the additional network parameters provided by the *correction unit*, then re-training the correction unit on the 50% least susceptible filter outputs should also achieve the same performance as that achieved by applying a *correction unit* on the 50% most susceptible filter outputs identified by the ranking metric. To this end, we also report the accuracy for correcting the outputs of the 48 least distortion susceptible filters in the first layer of a pre-trained AlexNet, represented by ranked\_48\_least in Figure 9. As shown in Figure 9, the performance of the ranked\_48\_least model is significantly poorer than the proposed ranked\_48 model, which corrects activations of the most susceptible filters. The ranked\_48\_least model can be seen as a lower bound on the accuracy of the random\_48 model, thus highlighting the importance of ranking filters in a convolutional layer on the basis of susceptibility to image distortions and correcting the most susceptible ones. As shown in Table 6, p-values for paired sample t-tests between random. $l$  and ranked. $l$  model performances are all lesser than 0.05, indicating the difference in accuracy is statistically significant.

## 5.2. ImageNet Analysis

### 5.2.1 Fine-tuned model

Since fine-tuning all layers of a DNN results in the best accuracy for fine-tuned models (Tables 3 and 4), we fine-tune all layers of the AlexNet model in Figure 3b on a mix of distortion affected images and clean images to generate a single fine-tuned model and refer to this model as Finetune-8 using the notation defined in Section 5.1. Similar to the fine-tuning procedure followed in Section 5.1, starting with an initial learning rate that is 10 times lower than that used to generate the pre-trained model in Figure 3b (0.001), momentum equal to 0.9 and batch size of 256, network parameters (60.94 million) are updated for a fixed number of

Table 7. Top-1 accuracy of various models for Gaussian blur affected images of the ImageNet validation set (ILSVRC2012). Bold numbers show best accuracy and underlined numbers show next best accuracy for each distortion level.

Method	Distortion Level							Avg	# Params (million)
	$\sigma_b = 0$	$\sigma_b = 1$	$\sigma_b = 2$	$\sigma_b = 3$	$\sigma_b = 4$	$\sigma_b = 5$	$\sigma_b = 6$		
Baseline	<u>0.5694</u>	0.4456	0.2934	0.1585	0.0786	0.0427	0.0256	0.2305	60.96
Finetune-8	0.5553	0.5301	0.5004	0.4669	0.4276	0.3886	0.3485	0.4596	60.96
Deepcorr-5c	0.5684	<u>0.5513</u>	<b>0.5300</b>	<b>0.5173</b>	<b>0.5011</b>	<b>0.4748</b>	<b>0.4519</b>	<b>0.5135</b>	61.44
Deepcorr-5	<b>0.5724</b>	<b>0.5522</b>	<u>0.5240</u>	<u>0.5100</u>	<u>0.4937</u>	<u>0.4643</u>	<u>0.4334</u>	<u>0.5071</u>	2.81
Deepcorr-5-no-bn	0.5647	0.5396	0.5000	0.4773	0.4524	0.4257	0.3921	0.4788	2.80
NCSR	<u>0.5694</u>	0.4553	0.2897	0.1263	0.0578	0.0259	0.0107	0.2193	-

Table 8. Top-1 accuracy of various models for AWGN affected images of the ImageNet validation set (ILSVRC2012). Bold numbers show best accuracy and underlined numbers show next best accuracy for each distortion level.

Method	Distortion Level							Avg	# Params (million)
	$\sigma_n = 0$	$\sigma_n = 10$	$\sigma_n = 20$	$\sigma_n = 40$	$\sigma_n = 60$	$\sigma_n = 80$	$\sigma_n = 100$		
Baseline	<u>0.5694</u>	0.5218	0.3742	0.1256	0.0438	0.0190	0.0090	0.2375	60.96
Finetune-8	0.5540	0.5477	0.5345	0.5012	0.4654	0.4297	0.3936	0.4894	60.96
Deepcorr-5c	0.5657	0.5598	0.5496	<b>0.5235</b>	<b>0.4942</b>	<b>0.4623</b>	<b>0.4320</b>	<b>0.5124</b>	61.44
Deepcorr-5	<b>0.5712</b>	<b>0.5660</b>	<b>0.5546</b>	<u>0.5213</u>	<u>0.4870</u>	<u>0.4509</u>	<u>0.4138</u>	<u>0.5092</u>	2.81
Deepcorr-5-no-bn	0.5663	0.5601	0.5463	0.5145	0.4791	0.4453	0.4076	0.5027	2.80
BM3D	<u>0.5694</u>	<u>0.5638</u>	<u>0.5539</u>	0.5113	0.4759	0.4435	0.4047	0.5032	-

iterations (62500 iterations  $\approx$  10 epochs), with the learning rate reduced by a factor of 10 after every 18750 iterations (roughly 3 epochs). We use a data augmentation method as proposed by He et al (2016).

### 5.2.2 DeepCorrect models

Our main *DeepCorrect* model for ImageNet shown in Figure 8b is generated by correcting  $\beta_i N_i$  ranked distortion susceptible filters in the first 5 layers out of the 8 layered pre-trained AlexNet DNN shown in Figure 3b and referred to as Deepcorr-5 in Tables 7-8, using the notation defined in Section 5.1. Deepcorr-5 is generated by correcting 75% ranked filter outputs in the first two layers ( $\beta_1, \beta_2 = 0.75$ ) and 50% ranked filter outputs in the next three layers ( $\beta_3, \beta_4, \beta_5 = 0.5$ ). The correction priority computed using Algorithm 1 is used to independently rank the distortion susceptible filters within each layer (local ranking) and correct the activations of the top  $\beta_i N_i$  filters in each layer. The *correction units* (Figure 7) in each convolutional layer are trained using an initial learning rate of 0.1 and the same learning rate schedule, data augmentation and total iterations used for generating the Finetune-8 model in Section 5.2.1. Additional details regarding the *correction unit* architecture for Deepcorr-5 can be found in Table 10. We also generate 2 additional variants based on our Deepcorr-5 model: 1) Deepcorr-5c, wherein parameters in the final three fully connected layers are also updated and 2) Deepcorr-5-no-bn, which is a Deepcorr-5 architecture without any batch normalization in

the *correction units*.

Tables 7-8 show the superior performance of our proposed method as compared to fine-tuning a model. The Deepcorr-5c model performs the best with a  $\approx$  12% and  $\approx$  5% average improvement relative to Finetune-8 for Gaussian blur and AWGN, respectively. Deepcorr-5c significantly improves the robustness of a pre-trained DNN achieving an average top-1 accuracy of 0.5135 and 0.5124 for Gaussian blur and AWGN affected images, respectively, as compared to the corresponding top-1 accuracy of 0.2305 and 0.2375 for the pre-trained AlexNet DNN. However, this requires training slightly more parameters than those trained for Finetune-8, whereas the Deepcorr-5 model is able to recover most of the performance lost by the baseline model, by just training  $\approx$  2.81 million parameters (95.4% lesser parameters than Finetune-8). The Deepcorr-5 model outperforms Finetune-8 with a  $\approx$  10% and  $\approx$  4% relative average improvement for Gaussian blur and AWGN, respectively. Figure 10 shows the t-SNE feature embedding of our Deepcorr-5 model features for classes shown in Figure 2. Unlike the clustering of classes in Figure 2, Deepcorr-5 features are discriminative enough to generate a concise clustering of images from the same class and also provide a good separation between clusters of other classes, even as distortion severity increases. Deepcorr-5's average performance is only 1.2% lower relative to Deepcorr-5c whilst training 96% lesser parameters than Deepcorr-5c, which indicates that most of the distortion invariance can be encoded in the earlier convolutional layers. All

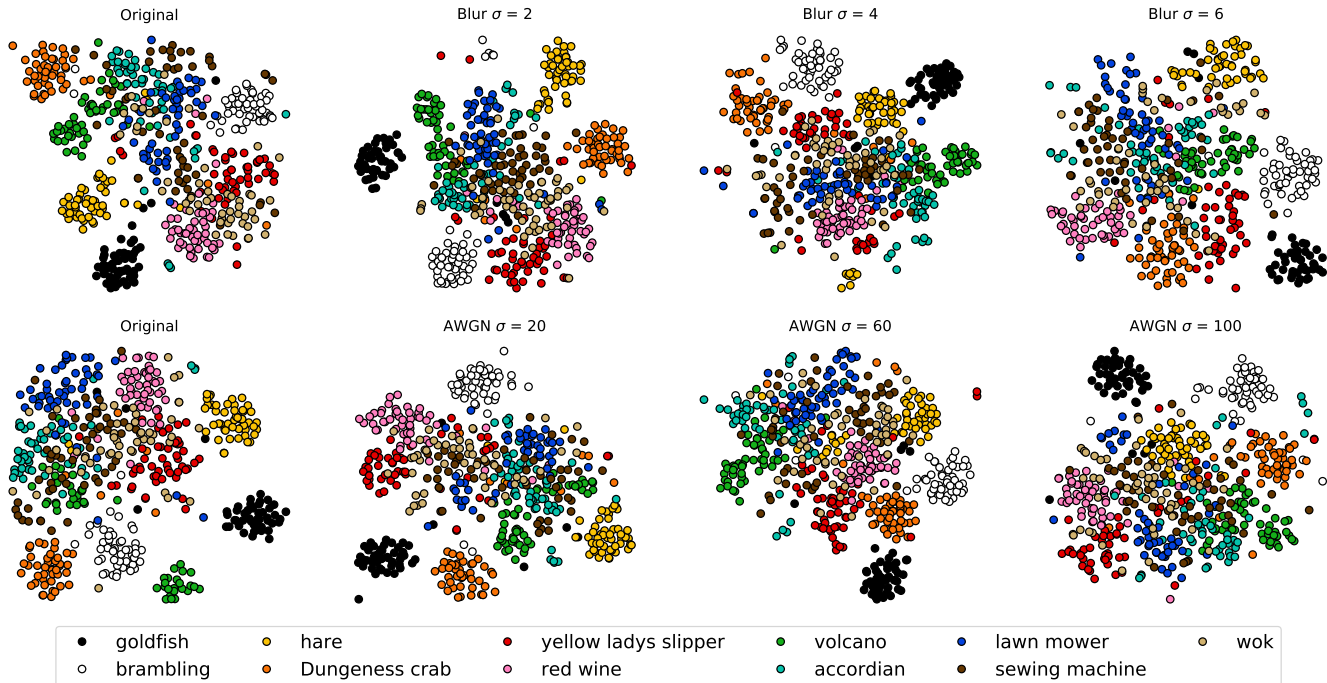


Figure 10. Two-dimensional t-SNE (Maaten and Hinton, 2008) embedding of the penultimate layer features of Deepcorr-5, visualized for original (undistorted), blurred and noise affected images for same 11 classes of the ILSVRC2012 dataset (Deng et al, 2009) visualized in Figure 2, with distortion severity increasing from left to right. **Top row:** embedding for Gaussian blur affected images. **Bottom row:** embedding for AWGN affected images (best viewed in color).

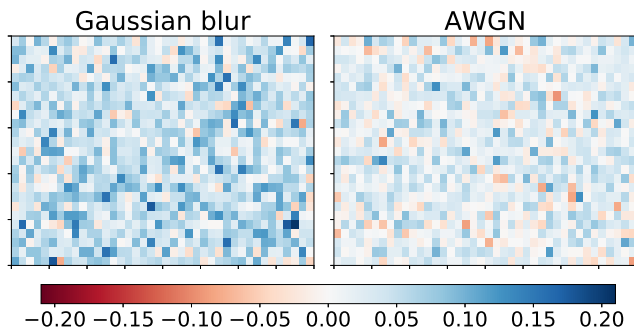


Figure 11. 2-D heat map of per-class accuracy difference between Deepcorr-5 model and Finetune-8 model for the ImageNet validation set. Each colored square in the heat map represents per-class accuracy difference for a particular class, with positive values in the heat map (blue) representing classes for which Deepcorr-5 outperforms Finetune-8 and negative values (red) representing the opposite. **Left:** per-class accuracy difference heat map for Gaussian blur, with Deepcorr-5 performing better for 865 classes, Finetune-8 performing better for 121 classes and both performing equally well for 14 classes. **Right:** per-class accuracy difference heat map for AWGN, with Deepcorr-5 performing better for 707 classes, Finetune-8 performing better for 257 classes and both performing equally well for 36 classes.

our Deepcorr-5 model variants consistently outperform the Finetune-8 model for both distortion types and all levels of distortion.

Table 9. Top-1 accuracy of the Deepcorr-5 model for the ImageNet validation set (ILSVRC2012), with filter outputs for correction chosen using either a local or global ranking approach. Performance is reported in terms of Top-1 accuracy averaged over all distortion levels, including original images.

Filter ranking	Gaussian blur	AWGN
Local	0.5071	0.5093
	# corrected per layer	# corrected per layer
	{72, 192, 192, 192, 128}	{72, 192, 192, 192, 128}
Global	0.5062	0.5087
	# corrected per layer	# corrected per layer
	{81, 128, 168, 207, 192}	{71, 150, 187, 193, 175}

We also look at the classification performance for Deepcorr-5 and Finetune-8 by plotting a 2-dimensional heat map of the per-class accuracy difference between Deepcorr-5 and Finetune-8, as shown in Figure 11. Each square in the heat map represents one class in ImageNet, with positive values in the heat map (blue) representing classes for which Deepcorr-5 outperforms Finetune-8 and negative values (red) representing the opposite. Deepcorr-5 not only outperforms Finetune-8 for most classes but also does so by a larger margin as compared to classes for which Finetune-8

outperforms Deepcorr-5. For completeness, we also compare classification performance with a commonly used non-blind image denoising method (BM3D) proposed by [Dabov et al \(2009\)](#) and a deblurring method (NCSR) proposed by [Dong et al \(2013\)](#) and report the corresponding Top-1 accuracy for these two methods in Tables 7-8, with the Deepcorr-5 model outperforming each for AWGN and Gaussian blur, respectively.

Finally in Table 9, we evaluate the effect of using a global ranking approach for Deepcorr-5, where we use the correction priority computed using Algorithm 1 to rank filters across all convolutional layers. By correcting the same number of total filter activations as the local ranking approach (776 filters out of 1376), we observe that the global ranking approach achieves an average accuracy similar to that of the local ranking approach. A paired sample t-test between the local and global ranking accuracies yielded a p-value of 0.8662 ( $> 0.05$ ), i.e. the difference between the global and local ranking accuracies was not statistically significant.

### 5.2.3 Correction unit architectures

Increasing the correction width ( $D_i$  in Figure 7) makes our proposed *correction unit* wider, whereas decreasing  $D_i$  makes the *correction unit* thinner. A natural choice for  $D_i$  would be to make it equal to the number of distortion susceptible filters that need correction ( $\beta_i N_i$ ), in a DNN layer  $i$ ; this is also the default parameter setting used in the *correction units* for Deepcorr-5, as shown in the first row of Table 10. We refer to such *correction units* as critically-wide (CW) *correction units*. Since the correction width is always equal to the number of distortion susceptible filters that need correction (i.e.  $D_i = \beta_i N_i$ ), the number of trainable parameters in the CW *correction units* of Deepcorr-5 scale linearly with the number of corrected filters ( $\beta_i N_i$ ) in each convolutional layer, even though Deepcorr-5 trains significantly lesser parameters than Finetune-8 and still achieves a better classification accuracy. Considering the practical constraints on time-complexity and memory usage while training/testing extremely deep networks like those proposed by [Simonyan and Zisserman \(2014\)](#), [Szegedy et al \(2015\)](#) and [He et al \(2016\)](#), training CW *correction units*, where correction width equals the number of filters that need correction (i.e.  $D_i = \beta_i N_i$ ), may not be economical.

One way to reduce the number of trainable parameters in *correction units* is to choose a single value for the correction width ( $D_i$ ) which keeps the number of trainable parameters low and also does not significantly reduce the learning capacity of the corresponding *DeepCorrect* models. An example of such a *correction unit* with lesser trainable parameters can be seen in row two of Table 10. Replacing each CW *correction unit* in Deepcorr-5 with such a computationally lite

*correction unit* results in a *DeepCorrect* model that updates lesser parameters than Deepcorr-5 and which we refer to as Deepcorr-5-lite (Table 10, row two). For Deepcorr-5-lite, correction width  $D_i$  is equal to 128 for  $1 \leq i \leq 5$ . Table 10 shows architecture details for Deepcorr-5 and Deepcorr-5-lite. As shown in Table 10, unlike the CW *correction units* of Deepcorr-5, the number of trainable parameters in each *correction unit* of Deepcorr-5-lite are approximately equal and do not increase as the number of filters corrected ( $\beta_i N_i$ ) increase, while going from conv-1 to conv- $n$ , where conv- $i$  is the  $i^{\text{th}}$  convolutional layer in an  $n$  layered DNN.

Another way to limit the number of trainable parameters and floating-point operations (FLOPs) is to explore a bottleneck architecture for our *correction units*, where the correction width  $D_i$  is set to 50% of the distortion susceptible filters that need correction in a DNN layer  $i$  ( $D_i = \frac{\beta_i N_i}{2}$ , i.e dimensionality reduction), along with an additional  $3 \times 3$  convolutional layer. Replacing each CW *correction unit* in Deepcorr-5 with such a bottleneck *correction unit* results in a *DeepCorrect* model that has significantly lesser trainable parameters and FLOPs than Deepcorr-5, which we refer to as Deepcorr-5-bottleneck (Table 10, row three).

We train Deepcorr-5-lite and Deepcorr-5-bottleneck using the same learning rate schedule and data augmentation used for Deepcorr-5 and report the top-1 accuracy on the ImageNet validation set in Tables 11 and 12. As shown in Tables 11 and 12, Deepcorr-5-lite is able to achieve almost the same average accuracy as Deepcorr-5, with a 41% reduction in trainable parameters and a 17.3% reduction in FLOPs, relative to Deepcorr-5. Similarly, Deepcorr-5-bottleneck achieves  $\approx 99\%$  of the average accuracy achieved by Deepcorr-5, with a 63% reduction in trainable parameters and a 73% reduction in FLOPs, relative to Deepcorr-5. As seen in Table 10, compared to Deepcorr-5-lite, Deepcorr-5-bottleneck trains 38% lesser parameters and performs 67% lesser FLOPs. From Tables 10-12, it is evident that Deepcorr-5-bottleneck provides the best trade-off between model capacity and computational complexity.

### 5.2.4 Accelerating training

We analyze the evolution of validation set accuracy over training iterations for four Deepcorr-5 model variants as well as the Finetune-8 model. As shown in Figure 12, all four Deepcorr-5 model variants not only achieve a final validation accuracy higher than the Finetune-8 model, but also train faster. For any particular value of validation accuracy achieved by the Finetune-8 model in Figure 12, all four Deepcorr-5 model variants are able to achieve the same validation accuracy with much lesser number of training iterations, with Deepcorr-5, Deepcorr-5-lite and Deepcorr-5-bottleneck being fastest, followed by Deepcorr-5-no-bn. Thus, we conclude that just learning corrective transforms

Table 10. Architecture details of *DeepCorrect* models for AlexNet, along with the number of trainable parameters for each model. The number following Corr-unit specifies the layer at which *correction units* are applied. *Correction unit* convolutional layers are represented as  $[k \times k, d]$ , where  $k \times k$  is the spatial extent of a filter and  $d$  is the number of filters in a layer.

Model	Corr-unit 1 $\beta_1 N_1 = 72$	Corr-unit 2 $\beta_2 N_2 = 192$	Corr-unit 3 $\beta_3 N_3 = 192$	Corr-unit 4 $\beta_4 N_4 = 192$	Corr-unit 5 $\beta_5 N_5 = 128$
Deepcorr-5	$\begin{bmatrix} 1 \times 1, 72 \\ 5 \times 5, 72 \\ 5 \times 5, 72 \\ 1 \times 1, 72 \end{bmatrix}$	$\begin{bmatrix} 1 \times 1, 192 \\ 3 \times 3, 192 \\ 3 \times 3, 192 \\ 1 \times 1, 192 \end{bmatrix}$	$\begin{bmatrix} 1 \times 1, 192 \\ 3 \times 3, 192 \\ 3 \times 3, 192 \\ 1 \times 1, 192 \end{bmatrix}$	$\begin{bmatrix} 1 \times 1, 192 \\ 3 \times 3, 192 \\ 3 \times 3, 192 \\ 1 \times 1, 192 \end{bmatrix}$	$\begin{bmatrix} 1 \times 1, 128 \\ 3 \times 3, 128 \\ 3 \times 3, 128 \\ 1 \times 1, 128 \end{bmatrix}$
# total params: $2.81 \times 10^6$	# params: 270,288	# params: 739,200	# params: 739,200	# params: 739,200	# params: 328,960
	# FLOPs: $8.16 \times 10^8$	# FLOPs: $5.38 \times 10^8$	# FLOPs: $1.24 \times 10^8$	# FLOPs: $1.24 \times 10^8$	# FLOPs: $5.54 \times 10^7$
Deepcorr-5-lite <sup>a</sup>	$\begin{bmatrix} 1 \times 1, 128 \\ 3 \times 3, 128 \\ 3 \times 3, 128 \\ 1 \times 1, 72 \end{bmatrix}$	$\begin{bmatrix} 1 \times 1, 128 \\ 3 \times 3, 128 \\ 3 \times 3, 128 \\ 1 \times 1, 192 \end{bmatrix}$	$\begin{bmatrix} 1 \times 1, 128 \\ 3 \times 3, 128 \\ 3 \times 3, 128 \\ 1 \times 1, 192 \end{bmatrix}$	$\begin{bmatrix} 1 \times 1, 128 \\ 3 \times 3, 128 \\ 3 \times 3, 128 \\ 1 \times 1, 192 \end{bmatrix}$	$\begin{bmatrix} 1 \times 1, 128 \\ 3 \times 3, 128 \\ 3 \times 3, 128 \\ 1 \times 1, 128 \end{bmatrix}$
# total params: $1.67 \times 10^6$	# params: 314,568	# params: 345,408	# params: 345,408	# params: 345,408	# params: 328,960
	# FLOPs: $9.49 \times 10^8$	# FLOPs: $2.51 \times 10^8$	# FLOPs: $5.82 \times 10^7$	# FLOPs: $5.82 \times 10^7$	# FLOPs: $5.54 \times 10^7$
Deepcorr-5-bottleneck <sup>a</sup>	$\begin{bmatrix} 1 \times 1, 36 \\ 3 \times 3, 36 \\ 3 \times 3, 36 \\ 3 \times 3, 36 \\ 1 \times 1, 72 \end{bmatrix}$	$\begin{bmatrix} 1 \times 1, 96 \\ 3 \times 3, 96 \\ 3 \times 3, 96 \\ 3 \times 3, 96 \\ 1 \times 1, 192 \end{bmatrix}$	$\begin{bmatrix} 1 \times 1, 96 \\ 3 \times 3, 96 \\ 3 \times 3, 96 \\ 3 \times 3, 96 \\ 1 \times 1, 192 \end{bmatrix}$	$\begin{bmatrix} 1 \times 1, 96 \\ 3 \times 3, 96 \\ 3 \times 3, 96 \\ 3 \times 3, 96 \\ 1 \times 1, 192 \end{bmatrix}$	$\begin{bmatrix} 1 \times 1, 64 \\ 3 \times 3, 64 \\ 3 \times 3, 64 \\ 3 \times 3, 64 \\ 1 \times 1, 128 \end{bmatrix}$
# total params: $1.03 \times 10^6$	# params: 40,680	# params: 287,040	# params: 287,040	# params: 287,040	# params: 127,872
	# FLOPs: $1.22 \times 10^8$	# FLOPs: $2.08 \times 10^8$	# FLOPs: $4.83 \times 10^7$	# FLOPs: $4.83 \times 10^7$	# FLOPs: $2.15 \times 10^7$

<sup>a</sup> We use a pair of dilated convolutions (Yu and Koltun, 2015) of size  $3 \times 3$  in place of a pair of traditional  $5 \times 5$  convolutions in Corr-unit 1, to generate an effective receptive field of size  $7 \times 7$ .

Table 11. Top-1 accuracy of *DeepCorrect* models with different *correction unit* architectures, for Gaussian blur affected images of the ImageNet validation set (ILSVRC2012). Bold numbers show best accuracy for each distortion level.

Method	Distortion Level							Avg	# Params (million)
	$\sigma_b = 0$	$\sigma_b = 1$	$\sigma_b = 2$	$\sigma_b = 3$	$\sigma_b = 4$	$\sigma_b = 5$	$\sigma_b = 6$		
Deepcorr-5	<b>0.5724</b>	<b>0.5522</b>	0.5240	<b>0.5100</b>	<b>0.4937</b>	<b>0.4643</b>	<b>0.4334</b>	<b>0.5071</b>	2.81
Deepcorr-5-lite	0.5718	0.5515	<b>0.5254</b>	0.5091	0.4899	0.4605	0.4270	0.5050	1.67
Deepcorr-5-bottleneck	0.5701	0.5504	0.5232	0.5070	0.4856	0.4560	0.4233	0.5022	1.03

Table 12. Top-1 accuracy of *DeepCorrect* models with different *correction unit* architectures, for AWGN affected images of the ImageNet validation set (ILSVRC2012). Bold numbers show best accuracy for each distortion level.

Method	Distortion Level							Avg	# Params (million)
	$\sigma_n = 0$	$\sigma_n = 10$	$\sigma_n = 20$	$\sigma_n = 40$	$\sigma_n = 60$	$\sigma_n = 80$	$\sigma_n = 100$		
Deepcorr-5	<b>0.5712</b>	<b>0.5660</b>	<b>0.5546</b>	<b>0.5213</b>	0.4870	<b>0.4509</b>	<b>0.4138</b>	<b>0.5092</b>	2.81
Deepcorr-5-lite	0.5711	<b>0.5660</b>	0.5527	0.5211	<b>0.4871</b>	0.4499	0.4125	0.5086	1.67
Deepcorr-5-bottleneck	0.5705	0.5649	0.5513	0.5191	0.4843	0.4456	0.4085	0.5063	1.03

for activations of a subset of convolutional filters in a layer accelerates training, with an additional speedup achieved by incorporating batch normalization in the correction units.

### 5.3. Generalization of DeepCorrect Features to other Datasets

To analyze the ability of distortion invariant features learnt for image classification to generalize to related tasks

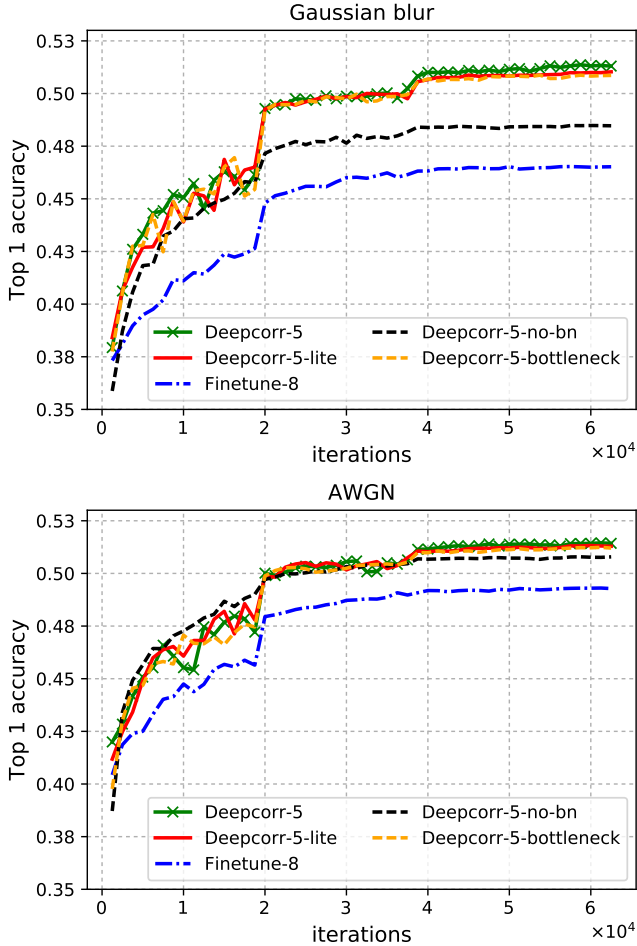


Figure 12. ImageNet validation set accuracy for *DeepCorrect* model variants and fine-tuning. **Top**: Accuracy vs. iterations for Gaussian blur. **Bottom**: Accuracy vs. iterations for AWGN.

like object recognition and scene recognition, we evaluate the Deepcorr-5, baseline AlexNet and Finetune-8 models trained on the ImageNet dataset (Section 5.2) as discriminative deep feature extractors on the Caltech-101, Caltech-256 and SUN-397 datasets. The Caltech-101 dataset consists of 101 object classes with a minimum of 40 images per class. The Caltech-256 dataset consists of 256 object classes with a minimum of 80 images per class. Unlike the task of object recognition, where the aim is to classify the main object in the image, the goal of scene recognition is to classify the entire scene of the image. Unlike object recognition datasets like Caltech-101 and Caltech-256, which bear some similarity to an image classification/object recognition dataset like ImageNet, a scene recognition dataset like SUN-397 bears no similarity to the ImageNet dataset and is expected to be very challenging for features extracted using models learnt on ImageNet (Donahue et al, 2014). The SUN-397 dataset consists of 397 scene categories with at least 100 images per class. Following the experimental procedure proposed by

Table 13. Mean accuracy per category of pre-trained AlexNet deep feature extractor for clean images.

Caltech-101	Caltech-256	SUN-397
0.8500	0.6200	0.3100

Table 14. Mean accuracy per category for Gaussian blur affected images, averaged over all distortion levels. Bold numbers show best accuracy.

Dataset	Baseline	Finetune-8	Deepcorr-5
Caltech-101	0.4980	0.7710	<b>0.8371</b>
Caltech-256	0.2971	0.5167	<b>0.5883</b>
SUN-397	0.1393	0.2369	<b>0.3049</b>

Table 15. Mean accuracy per category for AWGN affected images, averaged over all distortion levels. Bold numbers show best accuracy.

Dataset	Baseline	Finetune-8	Deepcorr-5
Caltech-101	0.3423	0.7705	<b>0.8034</b>
Caltech-256	0.1756	0.4995	<b>0.5482</b>
SUN-397	0.0859	0.1617	<b>0.2936</b>

Donahue et al (2014), we use the output of the first (Caltech-101 and Caltech-256) or second (SUN-397) fully-connected layer in these models as a deep feature extractor that can be used for object recognition and scene recognition in images affected by distortion.

Since the above deep feature models have not been trained on any one of these datasets (Caltech-101, Caltech-256 and SUN-397), for each dataset, we train linear SVMs on top of the deep features, which are extracted from a random set of training data, and evaluate the performance in terms of mean accuracy per category averaged over 5 data splits, following the training procedure adopted by Donahue et al (2014). The training data for each split consists of 25 training images and 5 validation images per class, sampled randomly from the considered dataset and all remaining images are used for testing. A baseline accuracy for undistorted images is first established by training linear SVMs on features extracted only from undistorted images using the AlexNet DNN shown in Figure 3b, and results are reported in Table 13.

Similar to the evaluation in Section 5.2, we now independently add Gaussian blur and AWGN to train and test images using the same distortion levels as used for the ImageNet dataset (Section 3) and report performance averaged over all distortion levels in Tables 14-15 for deep features extracted using baseline AlexNet, Finetune-8 and Deepcorr-5 models trained on ImageNet<sup>8</sup>.

Both Gaussian blur and AWGN significantly affect the accuracy of the baseline feature extractor for all three

<sup>8</sup>For each of the three models, a single set of linear SVMs is trained for images affected by different levels of distortion and also clean images.

datasets, with a 41% and 60% drop in respective accuracies for Caltech-101, a 52% and 71% drop in respective accuracies for Caltech-256, and a 55% and 72% drop in respective mean accuracy for SUN-397, relative to the benchmark performance for clean images. For Caltech-101, the Deepcorr-5 feature extractor outperforms the Finetune-8 feature extractor with a 8.5% and 4.2% relative improvement in mean accuracy for Gaussian blur and AWGN affected images, respectively. For Caltech-256, the Deepcorr-5 feature extractor outperforms the Finetune-8 feature extractor with a 13.8% and 9.7% relative improvement for Gaussian blur and AWGN, respectively. Similarly, features extracted using the Deepcorr-5 model significantly outperform those extracted using the Finetune-8 model for SUN-397, with a 28.7% and 81.5% relative improvement in mean accuracy for Gaussian blur and AWGN, respectively. The large performance gap between Deepcorr-5 and Finetune-8 feature extractors highlights the generic nature of distortion invariant features learnt by our *DeepCorrect* models.

## 6. Conclusion

Deep networks trained on pristine images perform poorly when tested on distorted images affected by image blur or additive noise. Evaluating the effect of Gaussian blur and AWGN on the activations of convolutional filters trained on undistorted images, we observe that select filters in each DNN convolutional layer are more susceptible to input distortions than the rest. We propose a novel objective metric to assess the susceptibility of convolutional filters to distortion and use this metric to identify the filters that maximize DNN robustness to input distortions, upon correction of their activations.

We design *correction units*, which are *residual blocks* that are comprised of a small stack of trainable convolutional layers and a single skip connection per stack. These *correction units* are added at the output of the most distortion susceptible filters in each convolutional layer, whilst leaving the rest of the pre-trained (on undistorted images) filter outputs in the network unchanged. The resultant DNN models which we refer to as *DeepCorrect* models, significantly improve the robustness of DNNs against image distortions and also outperform the alternative approach of network fine-tuning on common vision tasks like image classification, object recognition and scene classification, whilst training significantly less parameters and achieving a faster convergence in training. Fine-tuning limits the ability of the network to learn invariance to severe levels of distortion, and re-training an entire network can be computationally expensive for very deep networks. By correcting the most distortion-susceptible convolutional filter outputs, we are not only able to make a DNN robust to severe distortions, but are also able to maintain a very good performance on clean images.

Although we focus on image classification and object recognition, our proposed approach is generic enough to apply to a wide selection of tasks that use DNN models such as object detection (Girshick et al (2014), Everingham et al (2010)) or semantic segmentation (Lin et al (2014)).

## References

- Basu S, Karki M, Ganguly S, DiBiano R, Mukhopadhyay S, Gayaka S, Kannan R, Nemani R (2015) Learning sparse feature representations using probabilistic quadrees and deep belief nets. In: *Neural Processing Letters*, Springer, pp 1–13 3
- Chollet F (2015) Keras. <https://github.com/fchollet/keras> 1, 10
- Dabov K, Foi A, Katkovnik V, Egiazarian K (2009) BM3D image denoising with shape-adaptive principal component analysis. In: *Proc. Workshop on Signal Processing with Adaptive Sparse Structured Representations (SPARS09)* 10, 15
- Deng J, Dong W, Socher R, Li LJ, Li K, Fei-Fei L (2009) ImageNet: A large-scale hierarchical image database. In: *Proceedings of the IEEE Conference on Computer Vision and Pattern Recognition*, IEEE, pp 248–255 1, 2, 3, 4, 14
- Diamond S, Sitzmann V, Boyd SP, Wetzstein G, Heide F (2017) Dirty pixels: Optimizing image classification architectures for raw sensor data. CoRR abs/1701.06487, URL <http://arxiv.org/abs/1701.06487> 4
- Dodge S, Karam L (2016) Understanding how image quality affects deep neural networks. In: *Eighth International Conference on Quality of Multimedia Experience (QoMEX)*, pp 1–6 1, 3
- Donahue J, Jia Y, Vinyals O, Hoffman J, Zhang N, Tzeng E, Darrell T (2014) DeCAF: A deep convolutional activation feature for generic visual recognition. In: *International Conference on Machine Learning*, pp 647–655 17
- Dong W, Zhang L, Shi G, Li X (2013) Nonlocally centralized sparse representation for image restoration. In: *IEEE Trans. on Image Processing*, vol 22, pp 1620–1630 10, 15
- Everingham M, Van Gool L, Williams CKI, Winn J, Zisserman A (2010) The Pascal visual object classes (VOC) challenge. In: *International Journal of Computer Vision*, vol 88, pp 303–338 18
- Fei-Fei L, Fergus R, Perona P (2007) Learning generative visual models from few training examples: An incremental bayesian approach tested on 101 object categories. In: *Computer Vision and Image Understanding*, Elsevier, vol 106, pp 59–70, URL [http://www.vision.caltech.edu/Image\\_Datasets/Caltech101/](http://www.vision.caltech.edu/Image_Datasets/Caltech101/) 2
- Girshick R, Donahue J, Darrell T, Malik J (2014) Rich feature hierarchies for accurate object detection and semantic segmentation. In: *Proceedings of the IEEE Conference on Computer Vision and Pattern Recognition*, pp 580–587 1, 18

- Goodfellow IJ, Shlens J, Szegedy C (2014) Explaining and harnessing adversarial examples. arXiv preprint arXiv:1412.6572 [3](#)
- Griffin G, Holub A, Perona P (2007) Caltech-256 object category dataset URL [http://www.vision.caltech.edu/Image\\_Datasets/Caltech256/](http://www.vision.caltech.edu/Image_Datasets/Caltech256/) [2](#)
- He K, Zhang X, Ren S, Sun J (2016) Deep residual learning for image recognition. In: Proceedings of the IEEE Conference on Computer Vision and Pattern Recognition, pp 770–778 [1](#), [4](#), [8](#), [9](#), [10](#), [13](#), [15](#)
- Jia Y, Shelhamer E, Donahue J, Karayev S, Long J, Girshick R, Guadarrama S, Darrell T (2014) Caffe: Convolutional architecture for fast feature embedding. arXiv preprint arXiv:1408.5093 [1](#)
- Karahan S, Yildirim MK, Kirtac K, Rende FS, Butun G, Ekenel HK (2016) How image degradations affect deep CNN-based face recognition? In: *International Conference of the Biometrics Special Interest Group (BIOSIG)*, IEEE, pp 1–5 [3](#)
- Karam LJ, Zhu T (2015) Quality labeled faces in the wild (QLFW): a database for studying face recognition in real-world environments. In: *Proc. SPIE 9394, Human Vision and Electronic Imaging*, vol XX [3](#)
- Krizhevsky A, Hinton G (2009) Learning multiple layers of features from tiny images. Tech. rep., URL <https://www.cs.toronto.edu/~kriz/cifar.html> [2](#), [4](#)
- Krizhevsky A, Sutskever I, Hinton GE (2012) ImageNet classification with deep convolutional neural networks. In: *Advances in neural information processing systems*, pp 1097–1105 [1](#), [2](#), [5](#)
- Lenc K, Vedaldi A (2015) Understanding image representations by measuring their equivariance and equivalence. In: *Proceedings of the IEEE Conference on Computer Vision and Pattern Recognition*, pp 991–999 [3](#)
- Lin TY, Maire M, Belongie S, Hays J, Perona P, Ramanan D, Dollár P, Zitnick CL (2014) Microsoft COCO: Common objects in context. In: *European Conference on Computer Vision*, Springer, pp 740–755 [1](#), [18](#)
- Maaten L, Hinton G (2008) Visualizing data using t-SNE. *Journal of Machine Learning Research* 9(Nov):2579–2605 [1](#), [2](#), [3](#), [14](#)
- Nguyen A, Yosinski J, Clune J (2015) Deep neural networks are easily fooled: High confidence predictions for unrecognizable images. In: *Proceedings of the IEEE Conference on Computer Vision and Pattern Recognition (CVPR)*, pp 427–436 [3](#)
- Nilsback ME, Zisserman A (2008) Automated flower classification over a large number of classes. In: *Proceedings of the Indian Conference on Computer Vision, Graphics and Image Processing*, pp 722–729 [4](#)
- Ponomarenko N, Lukin V, Zelensky A, Egiazarian K, Carli M, Battisti F (2009) TID2008-A database for evaluation of full-reference visual quality assessment metrics. In: *Advances of Modern Radioelectronics*, vol 10, pp 30–45 [4](#)
- Redmon J, Divvala S, Girshick R, Farhadi A (2016) You only look once: Unified, real-time object detection. In: *Proceedings of the IEEE Conference on Computer Vision and Pattern Recognition*, pp 779–788 [1](#)
- Ren S, He K, Girshick R, Sun J (2015) Faster R-CNN: Towards real-time object detection with region proposal networks. In: *Advances in Neural Information Processing Systems*, pp 91–99 [1](#)
- Rodner E, Simon M, Fisher RB, Denzler J (2016) Fine-grained recognition in the noisy wild: Sensitivity analysis of convolutional neural networks approaches. arXiv preprint arXiv:1610.06756 [4](#)
- Rumelhart DE, Durbin R, Golden R, Chauvin Y (1995) Backpropagation. L. Erlbaum Associates Inc., Hillsdale, NJ, USA, chap Backpropagation: The Basic Theory, pp 1–34 [8](#)
- Simonyan K, Zisserman A (2014) Very deep convolutional networks for large-scale image recognition. *CoRR* abs/1409.1556, URL <http://arxiv.org/abs/1409.1556> [1](#), [4](#), [15](#)
- Springenberg JT, Dosovitskiy A, Brox T, Riedmiller M (2014) Striving for simplicity: The all convolutional net. arXiv preprint arXiv:1412.6806 [4](#), [5](#)
- Szegedy C, Zaremba W, Sutskever I, Bruna J, Erhan D, Goodfellow I, Fergus R (2013) Intriguing properties of neural networks. arXiv preprint arXiv:1312.6199 [3](#)
- Szegedy C, Liu W, Jia Y, Sermanet P, Reed S, Anguelov D, Erhan D, Vanhoucke V, Rabinovich A (2015) Going deeper with convolutions. In: *Proceedings of the IEEE Conference on Computer Vision and Pattern Recognition*, pp 1–9 [1](#), [15](#)
- Vasiljevic I, Chakrabarti A, Shakhnarovich G (2016) Examining the impact of blur on recognition by convolutional networks. *CoRR* abs/1611.05760, URL <http://arxiv.org/abs/1611.05760> [4](#), [10](#)
- Wah C, Branson S, Welinder P, Perona P, Belongie S (2011) The caltech-ucsd birds-200-2011 dataset. Tech Rep URL <http://www.vision.caltech.edu/visipedia/CUB-200.html> [4](#)
- Xiao J, Hays J, Ehinger KA, Oliva A, Torralba A (2010) Sun database: Large-scale scene recognition from abbey to zoo. In: *Proceedings of the IEEE Conference on Computer Vision and Pattern Recognition (CVPR)*, IEEE, pp 3485–3492 [2](#)
- Yu F, Koltun V (2015) Multi-scale context aggregation by dilated convolutions. *CoRR* abs/1511.07122, URL <http://arxiv.org/abs/1511.07122>, [1511.07122](#) [16](#)
- Zhou Y, Song S, Cheung NM (2017) On classification of distorted images with deep convolutional neural networks. arXiv preprint arXiv:1701.01924 [4](#)